Role of Atmosphere–Ocean–Ice Interaction in the Linkage between December Bering Sea Ice and Subsequent February Surface Air Temperature over North America

JIAZHEN ZHAO,[a] SHENGPING HE,[b,c,d] AND HUIJUN WANG[a,d,e]

[a] *Key Laboratory of Meteorological Disaster, Ministry of Education/Joint International Research Laboratory of Climate and Environment Change (ILCEC)/Collaborative Innovation Center on Forecast and Evaluation of Meteorological Disasters (CIC-FEMD), Nanjing University of Information Science and Technology, Nanjing, China*
[b] *Geophysical Institute, University of Bergen and Bjerknes Centre for Climate Research, Bergen, Norway*
[c] *Nansen Environmental and Remote Sensing Center, Bergen, Norway*
[d] *Nansen-Zhu International Research Centre, Institute of Atmospheric Physics, Chinese Academy of Sciences, Beijing, China*
[e] *Southern Marine Science and Engineering Guangdong Laboratory (Zhuhai), Zhuhai, China*

(Manuscript received 13 April 2022, in final form 31 October 2022)

ABSTRACT: This study revealed that the interannual variations of December Bering Sea ice and subsequent February surface air temperature (SAT) over North America are significantly correlated during 2000/01–2020/21, which is not the case during 1966/67–1999/2000. During 2000/01–2020/21, reduced December Bering Sea ice is generally followed by a February meridional dipole pattern in the atmospheric circulation over North America, which provides favorable conditions for colder temperatures. Further analysis elucidates that the intensified persistence of December Bering Sea ice anomaly might be responsible for the identified change in such a lead–lag sea ice–SAT linkage. During 2000/01–2020/21, the Bering Sea ice anomaly in December can persist into the subsequent February during which the sea ice anomaly exerts a thermal effect on the atmosphere aloft, stimulates an eastward-propagating Rossby wave train, and causes the meridional dipole pattern over North America. The longer persistence of December Bering Sea ice anomaly during 2000/01–2020/21 is attributed to the interdecadal intensified atmosphere–ocean–ice interaction over the Bering Sea—a positive feedback loop that favors the persistence of the sea ice anomaly. A negative sea ice concentration anomaly with more open water in the Bering Sea would allow the ocean to release more heat and warm more the air aloft. This will further lead to more downward longwave radiation, preventing the sea ice growth and helping maintain the sea ice anomaly. Results of this study indicates that the intensity of atmosphere–ocean–ice interaction in the Bering Sea may modulate the linkage between the February SAT over North America and the preceding December Bering Sea ice.

KEYWORDS: North America; Sea ice; Atmosphere-ocean interaction; Feedback; Surface fluxes; Temperature

1. Introduction

The latest study has indicated that the Arctic has warmed nearly 4 times faster than the global average since 1979 (Rantanen et al. 2022). This enhanced warming has been termed as Arctic amplification (AA) (Arrhenius 1897; Cohen et al. 2020). AA is strongest in winter, especially over areas with large sea ice loss (Screen and Simmonds 2010; Dai et al. 2019). In contrast to the AA and rapid warming over most of the world during the recent decades, numerous studies have noted an unexpected phenomenon that the winter temperature in the Northern Hemispheric midlatitudes has reversed its longer-term increasing trends to significant cooling trends from the late 1980s through to the early 2010s (Cohen et al. 2012, 2014; Sun et al. 2016; Xie et al. 2022; Ye et al. 2018). Such a winter cooling is linked to damaging extreme cold events in the Northern Hemispheric midlatitudes during recent years (Blackport et al. 2022; Johnson et al. 2018; Orsolini et al. 2016; Palmer 2014; Van Oldenborgh et al. 2015; Wallace et al. 2014). The cause of this unusual cooling and these frequent cold events has attracted considerable attention in the climate research community, yet it is still intensely debated (Blackport and Screen 2020; Cohen et al. 2021; Dai and Song 2020; Fischer and Knutti 2014; Francis 2017; Francis and Vavrus 2015; Screen and Simmonds 2014). Some studies attributed this cooling to the AA and the sea ice loss in the Arctic (Chen and Luo 2017; Francis et al. 2018; Liu et al. 2012; Mori et al. 2014, 2019; Overland et al. 2015; Wegmann et al. 2018), whereas some other studies attributed it to internal natural variability (Dai and Deng 2022; Li et al. 2015; Luo et al. 2017; McCusker et al. 2016).

North America is a typical region that has experienced dramatic cooling in winters during 1997/98–2013/14 (Cohen et al. 2014; Kug et al. 2015). Such winter cooling is accompanied by a series of unusually harsh cold winters such as the winters of 2009/10, 2010/11, and 2013/14, which cause considerable economic losses and casualties (Francis and Vavrus 2015; Orsolini et al. 2016). The atmospheric variability due to Arctic warming has been regarded as one of the causes of these severe winters (Cohen et al. 2018; Francis and Vavrus 2015; Screen and Simmonds 2014). It is suggested that regional warming in the Arctic and the associated changes of boundary forcing (e.g., changes in sea ice and snow cover) can contribute to colder winters in North America (Chen and Luo 2017; Kug et al. 2015; Zhang et al. 2020). As indicated by Kug et al. (2015), the cooling in North America can be attributed to

Denotes content that is immediately available upon publication as open access.

Corresponding author: Shengping He, Shengping.He@uib.no

DOI: 10.1175/JCLI-D-22-0265.1

© 2023 American Meteorological Society. For information regarding reuse of this content and general copyright information, consult the AMS Copyright Policy (www.ametsoc.org/PUBSReuseLicenses).

Brought to you by UNIVERSITETSBIBLIOTEKET I | Unauthenticated | Downloaded 04/25/23 11:32 AM UTC

warming and/or sea ice loss in East Siberian–Chukchi Sea region which could induce a downstream teleconnection pattern. In addition, more frequent high-latitude blocking, such as the Greenland blocking linked to regional and amplified warming in and around Greenland, is associated with the severe winters (e.g., cold temperatures, heavy snowfalls) over eastern North America (Chen and Luo 2017; Cohen et al. 2018; Hanna et al. 2018). Moreover, since blocking events herald sudden stratospheric warmings (SSWs) (Quiroz 1979, 1986), it is suggested that the SSWs favor surface cold spells over North America at the subseasonal time scale in the presence of low sea ice in the Barents–Kara Seas (Zhang et al. 2020). However, it still remains unclear if the Arctic change can significantly and physically affect the winter climate over North America (Blackport and Screen 2021; Blackport et al. 2019, 2022; Sigmond and Fyfe 2016). Previous studies have mainly investigated the winter (refers to December–February generally) mean SAT over North America; however, investigation into the monthly mean SAT remains insufficient. In fact, evidence suggests that the variability of monthly mean SAT might be totally different from that of the seasonal mean SAT at the Northern Hemispheric midlatitudes (Si et al. 2016; Wang et al. 2015). It indicates the necessity to conduct more research on the variability of monthly mean SAT over North America.

Cohen et al. (2014) have concluded three main dynamic pathways linking the Arctic warming to midlatitude weather: storm tracks, jet stream, and planetary wave propagations. The westerly jet stream, and especially its wavier track, has drawn most attention to explain the extreme cold winters in the Northern Hemispheric midlatitudes (Francis and Vavrus 2012, 2015; Martin 2021; Voosen 2021). Modeling studies indicate that the increased waviness of westerly jet streams that triggered the extreme weather over North America during the winter of 2013/14 is attributed to the reduced sea ice cover in the Bering Sea (Lee et al. 2015). In recent years, the climate linkage to the Bering Sea ice has gained wide attention. It is suggested that the variability of Bering Sea ice is closely tied to the Northern Hemispheric midlatitude climate (Iida et al. 2020; Tian et al. 2021; Zhuo and Jiang 2020; Zhou and Wang 2014). Loss of Bering Sea ice in the melt season (e.g., March–June) can cause an increase in the summertime (June–August) rainfall over the Lake Baikal area and northeastern China (Tian et al. 2021). In addition, Bering Sea ice anomalies in late winter can strengthen the North Pacific Oscillation in spring, which may further increase the maize/rice yields in northeastern China (Zhou and Wang 2014). Blackport et al. (2019) show that reduced Bering Sea ice is coincident with North American cold winters during the past decades. However, it has been argued that such a linkage might not be causal, and both of them are likely to be induced by the atmospheric internal variability (Blackport et al. 2019; Zhuo and Jiang 2020), for example, the Alaska Oscillation, which represents a dominant mode of sea level pressure variations over Alaska (Iida et al. 2020).

Previous studies have mainly focused on the linkage of winter mean Bering Sea ice with the simultaneous SAT over North America. Their linkage on the monthly time scale remains largely unexplored, which, however, might show distinct features from those obtained from the seasonal mean. Due to the intrinsic persistence of Bering Sea ice anomaly, there might be a significant lead–lag linkage of Bering Sea ice with the subsequent SAT over North America. Investigation into such a lead–lag linkage at monthly time scale might help for the short-term climate prediction.

2. Data and methods

Monthly atmospheric fields at a 2.5° × 2.5° resolution, monthly sea ice concentration (SIC), sea surface temperature (SST), surface sensible and latent heat fluxes (SHF and LHF; positive downward), surface downward longwave radiation, and surface net longwave radiation (positive downward) at a 0.25° × 0.25° resolution were obtained from the European Centre for Medium-Range Weather Forecasts (ECMWF) fifth-generation global atmospheric reanalysis (ERA5; Hersbach et al. 2020). Reanalysis data are currently available from January 1950 to the present. Surface turbulent heat flux (THF) denotes the sum of the SHF and the LHF, thereby positive value indicates downward. Given that ERA5 has only provided the surface downward longwave radiation and the surface net longwave radiation, we estimated the surface upward longwave radiation as the difference between the surface downward longwave radiation and the surface net longwave radiation (former minus latter). Note that positive values of the difference indicate longwave radiation from surface upward to atmosphere. Monthly snow cover extent was obtained from the Rutgers University Global Snow Laboratory (GSL), which is available from November 1966 to May 2021 with a spatial resolution of 190.6 km × 190.6 km at 60° latitude (Estilow et al. 2015; Robinson et al. 2012). Values are on an 88 × 88 subset of the original 89 × 89 matrices so that data only for grid cells that lie entirely within the Northern Hemisphere are provided. The observed east Pacific–North Pacific (EP-NP) index, which is used to characterize the atmospheric teleconnection pattern associated with the December Bering Sea ice anomaly, was obtained from the NOAA Climate Prediction Center (CPC) website.

The statistical methods of correlation, composite, and linear regression analysis are utilized to analyze the above data. To emphasize the interannual variability, linear trend has been removed prior to the analysis from all data (unless stated otherwise; i.e., Figs. 1, 2, 3a,b, 8, and 9). The annual cycle has been removed prior to the regression analysis. The statistical significance of the correlation is evaluated using the two-tailed Student's t test, with the effective degree of freedom N_e calculated as follows:

$$N_e = N_o \frac{1 - r_1 r_2}{1 + r_1 r_2}, \tag{1}$$

where N_o is the sample size, and r_1 and r_2 are autocorrelation coefficients at one time interval of the two series (Bretherton et al. 1999). All indices (e.g., sea ice index, the EP-NP index, etc.) in the current research were standardized. To diagnose the Rossby wave propagation, the wave activity flux (WAF) is applied in this study (Takaya and Nakamura 2001). An

Brought to you by UNIVERSITETSBIBLIOTEKET I | Unauthenticated | Downloaded 04/25/23 11:32 AM UTC

empirical orthogonal function (EOF) analysis (Chen et al. 2015) is conducted to characterize the spatiotemporal variability of December Bering Sea ice. In consideration of the temporal coverage of all the datasets, the analysis period is determined as 1966/67–2020/21.

3. The statistical linkage between December Bering Sea ice and subsequent February SAT over North America

Amidst rising global mean temperatures, the counterintuitive cooling trend across the Northern Hemispheric midlatitudes prevailed from the late 1980s through to the early 2010s (Fig. 1a). However, such a winter mean cooling trend has not continued over the past decade (Fig. 1b), which has also been indicated by Blackport and Screen (2020). Interestingly, notable discrepancies appear between the linear trends of the monthly mean and the seasonal mean SAT over North America from the late 1980s to the present (Figs. 1b–e). The trend map shown in Fig. 1e exhibits a counterintuitive decreasing trend of February SAT over North America during the past three decades. Therefore, the variability of February SAT over North America will be further investigated in this study. In addition, as motivated by previous studies (Iida et al. 2020; Tian et al. 2021; Zhuo and Jiang 2020; Zhou and Wang 2014), the potential impact of the SIC anomaly in the Bering Sea region is also the focus of this study. The Bering Sea keeps nearly ice free until the late fall (i.e., November) in the Pacific regions (Fig. 2a; 55°–65°N, 165°E–155°W; black rectangles in Fig. 2) where dramatic ice growth emerges during the early winter (i.e., December) (red contour in Fig. 2b). Correspondingly, this study will start the investigation with the lead–lag connection between February SAT over North America and the preceding December Bering Sea ice.

We first investigate the spatiotemporal characteristic of Bering Sea ice in December by applying an EOF analysis on the December SIC over the Bering Sea region (black rectangles in Fig. 2), and the results are shown in Figs. 3a and 3b. The first mode, which is significant and explains most of the total variance (62.6%), is dominated by variance in the northern part of the Bering Sea (i.e., around 60°–65°N; see Fig. 3a). Based on the spatial pattern shown in Fig. 3a, we define a Bering Sea ice index (SICBSI) as the area-averaged SIC over the region with the largest variance (60°–65°N, 165°–180°W; black rectangle in Fig. 3a). The SIC has been multiplied by −1 in defining the SICBSI so that a larger value of SICBSI indicates less SIC. To examine how much such a regional sea ice index can represent the variability of the Bering Sea ice, the time series of the December SICBSI (Fig. 3b, blue curve) is further compared with the time series of the principal component (PC) corresponding to the first EOF mode (Fig. 3b; red curve). In addition, the time series of area-averaged SIC over larger region of Bering Sea (i.e., 55°–65°N, 165°E–155°W; note that SIC is multiplied by −1) is also shown in Fig. 3b (orange curve). It is notable that all the three time series shown in Fig. 3b are well consistent with each other (with a correlation coefficient of 0.99). The results reasonably indicate that the December SICBSI can represent well the variability of the Bering Sea ice in December. Additionally, these time series show consistently an increasing trend since the 1990s, indicating a dramatic sea ice decline. In addition, the interannual variability of the Bering Sea ice in December has weakened since the year of 2000 (Fig. 3b), which might change its climatic linkage.

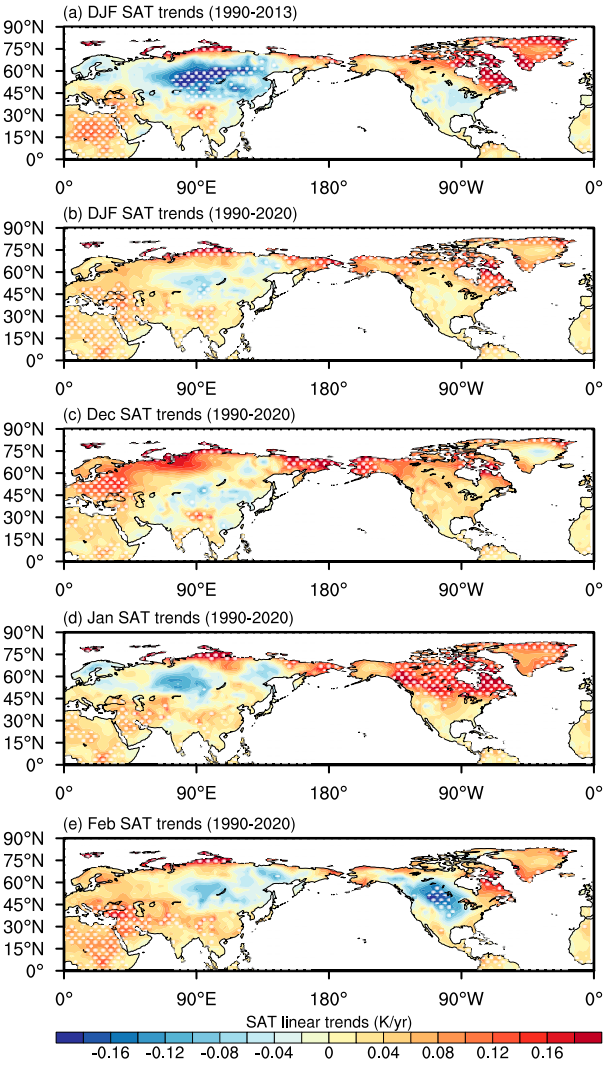

FIG. 1. Spatial patterns of linear trends of winter [December–February (DJF)] mean SAT (K yr^{-1}) during (a) 1990/91–2013/14 and (b) 1990/91–2020/21. (c)–(e) As in (b), but show the linear trends of monthly mean SAT in December, January, and February, respectively. Regions with white dots indicate that the trends are significant at the 90% confidence level.

Figure 3c shows the regressions of February SAT during 1967–2021 upon the December SICBSI during 1966–2020. Associated with below-normal Bering Sea ice in December, significantly negative SAT anomalies appear over North America (mainly in Alaska and northern Canada) in the subsequent February, indicating a significant lagged sea ice–SAT relationship. Based on the regressions shown in Fig. 3c, we define a North American SAT index (SATNAI) as the area-averaged SAT over the region 45°–70°N, 90°–165°W (black dashed rectangle in Fig. 3c). Standardized and linearly

Brought to you by UNIVERSITETSBIBLIOTEKET I | Unauthenticated | Downloaded 04/25/23 11:32 AM UTC

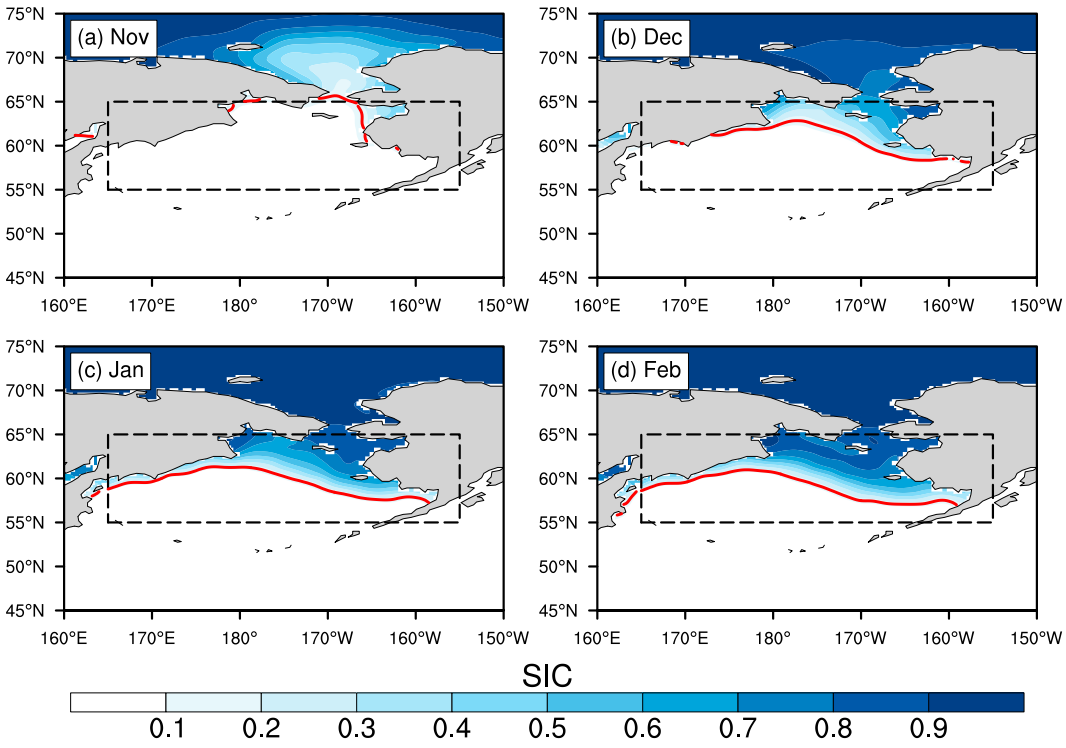

FIG. 2. Spatial patterns of climatology of the monthly mean SIC in (a) November, (b) December, (c) January, and (d) February during 1966/67–2020/21. The red contour in each panel represents the ice edge that is represented by a SIC value of 0.15. The black dashed rectangle (55°–65°N, 165°E–155°W) represents the Bering Sea region focused on in this study.

detrended time series of the December SICBSI and the February SATNAI are shown in Fig. 4a. As expected, the correlation coefficient between the SICBSI and SATNAI is −0.42, significant at 99% confidence level. The 9-yr low-pass filtered series implies that such an out-of-phase relationship tends to be unstable (Fig. 4a; dashed curves). Evidence suggested that the relationship between climatic systems could exhibit a significant interdecadal shift at a certain time point (Liu and He 2020; Xie et al. 2019; Xu et al. 2019). Therefore, a sliding correlation analysis is utilized to examine the change of the relationship between the December SICBSI and the February SATNAI (Fig. 4b). It is clear that their linkage has significantly intensified after the late 1990s. More specifically, an intensification occurs around the year of 2000. Accordingly, we divide the period 1966/67–2020/21 into two subperiods: 1966/67–1999/2000 and 2000/01–2020/21 (referred to as P1 and P2 hereafter, respectively). The correlation coefficient between the December SICBSI and the February SATNAI is changed from −0.35 (significant at 95% confidence level) during P1 to −0.58 (significant at 99% confidence level) during P2.

To further investigate the strengthening of the aforementioned lagged sea ice–SAT linkage, we show in Fig. 5 the February SAT (shading in Figs. 5a,b)/850-hPa horizontal wind (UV850; vectors in Figs. 5a,b) and February 500-hPa geopotential height (GPH500; shading in Figs. 5c,d) anomalies regressed upon the December SICBSI in the two subperiods. In Figs. 5c and 5d, the corresponding horizontal WAFs are also shown (vectors). During P1, the UV850 field displays an anomalous cyclone over Alaska (Fig. 5a; vectors), accompanied by significant cold anomalies near the surface (Fig. 5a; shading). Except for the anomalous low pressure around Alaska, the large-scale GPH500 field displays mostly insignificant anomalies over the North Pacific–North Atlantic sector (Fig. 5c; shading). The weak downstream propagation of WAFs shown in Fig. 5c (vectors) suggests that the GPH500 anomalies over North America may be developed by some perturbations over the high latitudes of North Pacific region. It is clear that the linkage between December Bering Sea ice and subsequent February North American SAT becomes more intense and significant during P2 (Fig. 5b). During P2, at 850 hPa, a large amount of significantly anomalous northerlies, which promote cold air intruding southward, pours into central North America from the Arctic and turns to the east (Fig. 5b; vectors). This leads to extensive and significant cold anomalies appearing over the central and eastern part of North America (Fig. 5b; shading). In the large-scale GPH500 field, significantly positive GPH anomalies appear over the high latitudes of the North Pacific region, together with alternating negative and positive GPH anomalies downstream (Fig. 5d; shading). Such a large-scale circulation pattern indicates an apparent Rossby wave train propagating from the high latitudes of North Pacific across northern North America toward southern North America.

Brought to you by UNIVERSITETSBIBLIOTEKET I | Unauthenticated | Downloaded 04/25/23 11:32 AM UTC

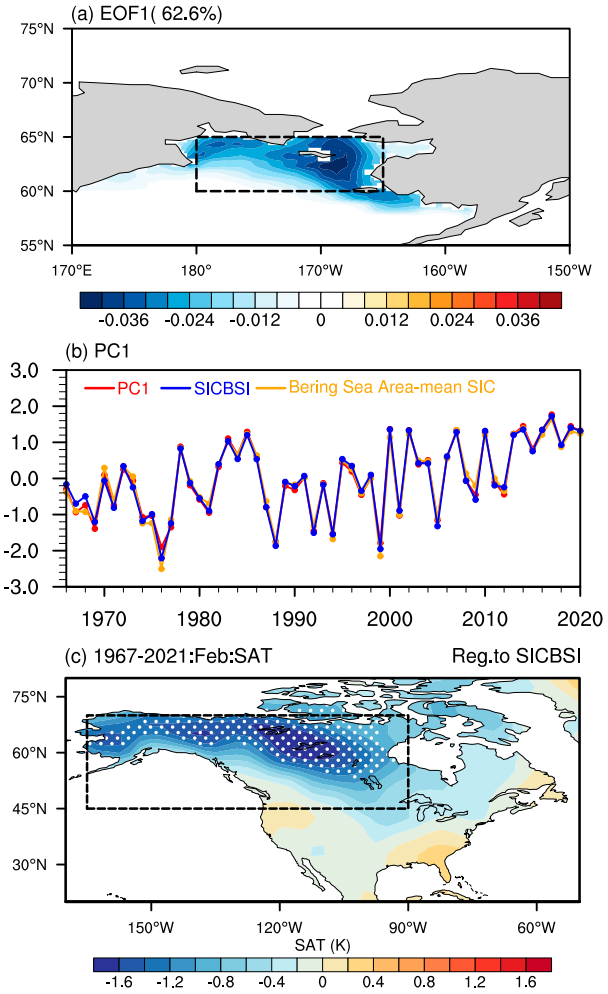

FIG. 3. (a) Spatial pattern of the first leading EOF mode of the variability of December Bering Sea ice. The black dashed rectangle indicates the region based on which the SICBSI is defined. (b) Standardized time series of the corresponding PC1 (red curve), the December area-averaged negative SIC (i.e., the SIC is multiplied by −1) in the domains 60°–65°N, 165°W–180° (i.e., the SICBSI; blue curve) and 55°–65°N, 165°E–155°W (orange curve) during 1966–2020. The results shown in (a) and (b) have not been linearly detrended. (c) Regressions of February SAT during 1967–2021 with respect to the December SICBSI during 1966–2020. Dotted areas indicate that the values are significant at the 95% confidence level. The black dashed rectangle marks the region used to define the SATNAI.

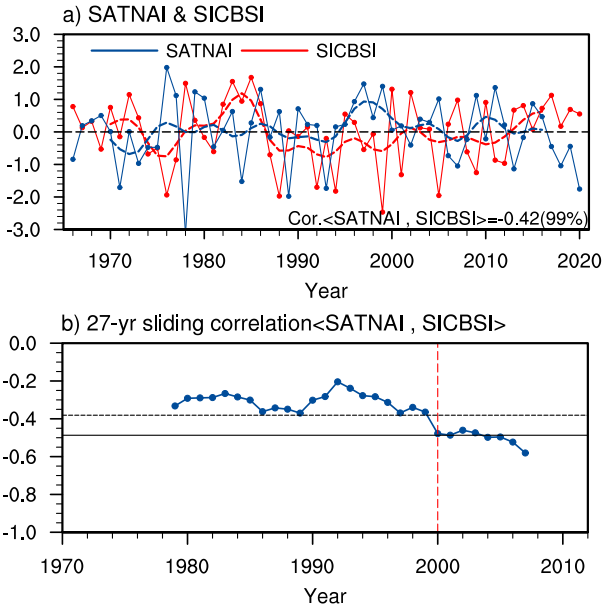

FIG. 4. (a) Standardized and linearly detrended time series of the December SICBSI (red solid curve) and the February SATNAI (blue solid curve) during 1966/67–2020/21. The dashed curves represent the 9-yr low-pass filtered series. (b) The 27-yr sliding correlation coefficients between the linearly detrended December SICBSI and February SATNAI during 1966/67–2020/21. The dashed and solid horizontal lines indicate the values significant at the 95% and 99% confidence levels, respectively. The vertical red dashed line indicates the year of 2000.

It then ramifies into two branches: one propagates southward toward lower latitudes, and the other propagates northward back toward the northern part of North America (Fig. 5d; vectors). The direction of the WAFs over the central part of North America in combination with that of the WAFs over the western North Atlantic suggests a potential interaction across circulation systems at mid–high latitudes. The more significant February circulation anomalies over North America in P2 than in P1, which are associated with reduced December SIC in the Bering Sea, explain well the aforementioned strengthening of the lagged sea ice–SAT linkage. In addition, the comparison of February large-scale atmospheric patterns during P1 (Fig. 5c) and P2 (Fig. 5d), which are associated with the reduced Bering Sea ice in the preceding December, indicates that the interdecadal intensified sea ice–SAT linkage is mainly attributed to the change in the teleconnections associated with the December Bering Sea ice anomaly.

4. Mechanism of the changed impacts of December Bering Sea ice

The analysis in section 3 reveals a significantly intensified interannual relationship between December Bering Sea ice and subsequent February North American SAT during P2. We next investigate the possible physical mechanisms underlying such an intensified connection. The intrinsic persistence of Bering Sea ice anomaly provides physical insight into the causes of the strengthening of the statistical sea ice–SAT linkage. We suspect that the significantly statistical sea ice–SAT linkage during P2 may result from that the Bering Sea ice anomaly in December persists into the subsequent February and then causes simultaneous SAT anomalies over North America. To test this idea, in the following analysis, we will mainly focus on the following two questions: 1) Is there any difference in the persistence of December Bering Sea ice anomaly between the two subperiods? 2) If the Bering Sea ice anomaly in December could persist into the subsequent

Brought to you by UNIVERSITETSBIBLIOTEKET I | Unauthenticated | Downloaded 04/25/23 11:32 AM UTC

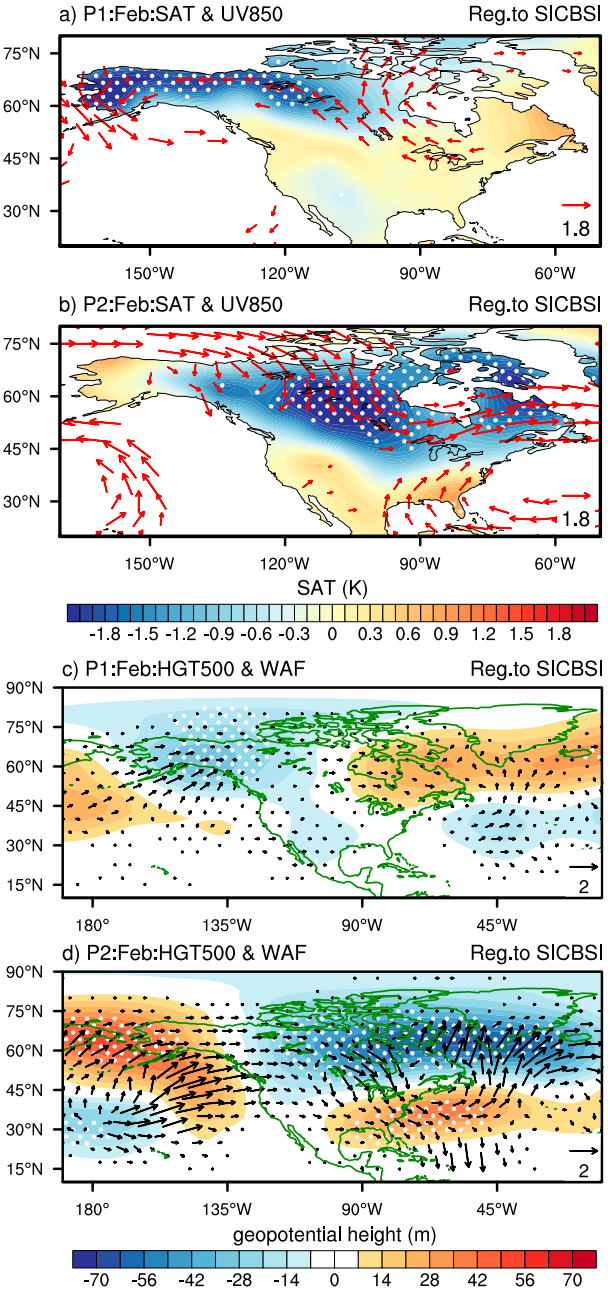

FIG. 5. (a),(b) Regressions of February SAT (shading) and UV850 (vectors) with respect to the December SICBSI during P1 and P2, respectively. The vectors shown are significant at the 95% confidence level. (c),(d) Regressions of February GPH500 (shading) with respect to the December SICBSI during P1 and P2, respectively, with the corresponding horizontal WAFs (vectors). Dotted areas in each panel indicate that the shading values are significant at the 95% confidence level.

February, how does the sea ice anomaly affect the SAT over remote areas in the North America?

Previous studies suggest that the intrinsic persistence of oceanic anomalies might play a central role in the lead–lag connections between climate variables (Li et al. 2021; McKinnon et al. 2016; Vijverberg and Coumou 2022; Yu and Sun 2021). Therefore, we first investigate the persistence of the December Bering Sea ice anomaly through regressing the monthly mean SIC in December, January, and February over the Bering Sea region upon the December SICBSI (Fig. 6; shading). Negative values indicate that the SIC in the northern part of the Bering Sea is lower than normal (Figs. 6a,d; shading). In the two subperiods, the December Bering Sea ice anomalies can persist into the following January (Figs. 6b,e; shading). In February, the situation becomes much different between the two subperiods. That is, the significant SIC anomaly can well persist into the following February during P2 (Fig. 6f; shading), which is not the case during P1 (Fig. 6c; shading). It indicates clearly that Bering Sea ice anomaly in December has longer persistence during P2 than during P1.

Previous studies indicate that extremely cold winters in North America may be attributed to the simultaneous low SIC in the Bering Sea (Iida et al. 2020; Lee et al. 2015; Nakanowatari et al. 2015). We further investigate whether the significantly negative Bering Sea ice anomaly in February during P2 leads to the simultaneous North American colder temperatures. In winter, sea ice reductions induced by a positive SST anomaly allows the warm ocean to release more heat to warm up the atmosphere aloft, leading to an increase in the upward THF at the surface (Dai et al. 2019; Deser et al. 2010). This can cause large-scale atmospheric circulation anomalies, having remote impacts (Cohen et al. 2014). On the other hand, sea ice reductions can serve as a response to the atmospheric forcing (Park et al. 2015). For example, sea ice reductions can be induced by warm air from the lower latitudes, which can cause an increase in the surface downward longwave radiation and the surface downward THF. Therefore, analysis of the simultaneous relationship between the anomalies of the SIC and the surface THF in situ can provide physical insight into the predominant direction of the atmosphere–ocean–ice interaction, which can indicate if the sea ice physically drives the atmospheric circulation aloft. That is, an in-phase relationship between the anomaly of the SIC and the THF (positive THF anomaly indicates downward) implies that the SIC anomaly drives the atmosphere and an out-of-phase relationship indicates the driving effects of atmosphere on the SIC anomaly. As shown in Fig. 6f (contours), associated with reduced December SIC in the Bering Sea, negative SIC anomalies in the Bering Sea concur with negative surface THF anomalies in situ in February during P2, showing an in-phase relationship between the anomaly of the SIC and the THF. Such an in-phase relationship indicates that the Bering Sea ice anomaly in February during P2 drives the atmospheric variability aloft, providing a prerequisite for the SIC anomaly to affect the large-scale atmospheric circulation and the SAT over North America. Based on the SIC anomaly pattern shown in Fig. 6f, we define a February Bering Sea ice index (Feb-SICBSI) as the area-averaged negative SIC (i.e., multiplied by −1) over the region of (57°–65°N, 177°E–165°W) (black dashed rectangle in Fig. 6f). Note that a larger value of Feb-SICBSI indicates less SIC. Figure 7a illustrates the regressions of February GPH500 (shading) upon the Feb-SICBSI during P2 with the corresponding horizontal WAFs (vectors). Corresponding to below-normal

Brought to you by UNIVERSITETSBIBLIOTEKET I | Unauthenticated | Downloaded 04/25/23 11:32 AM UTC

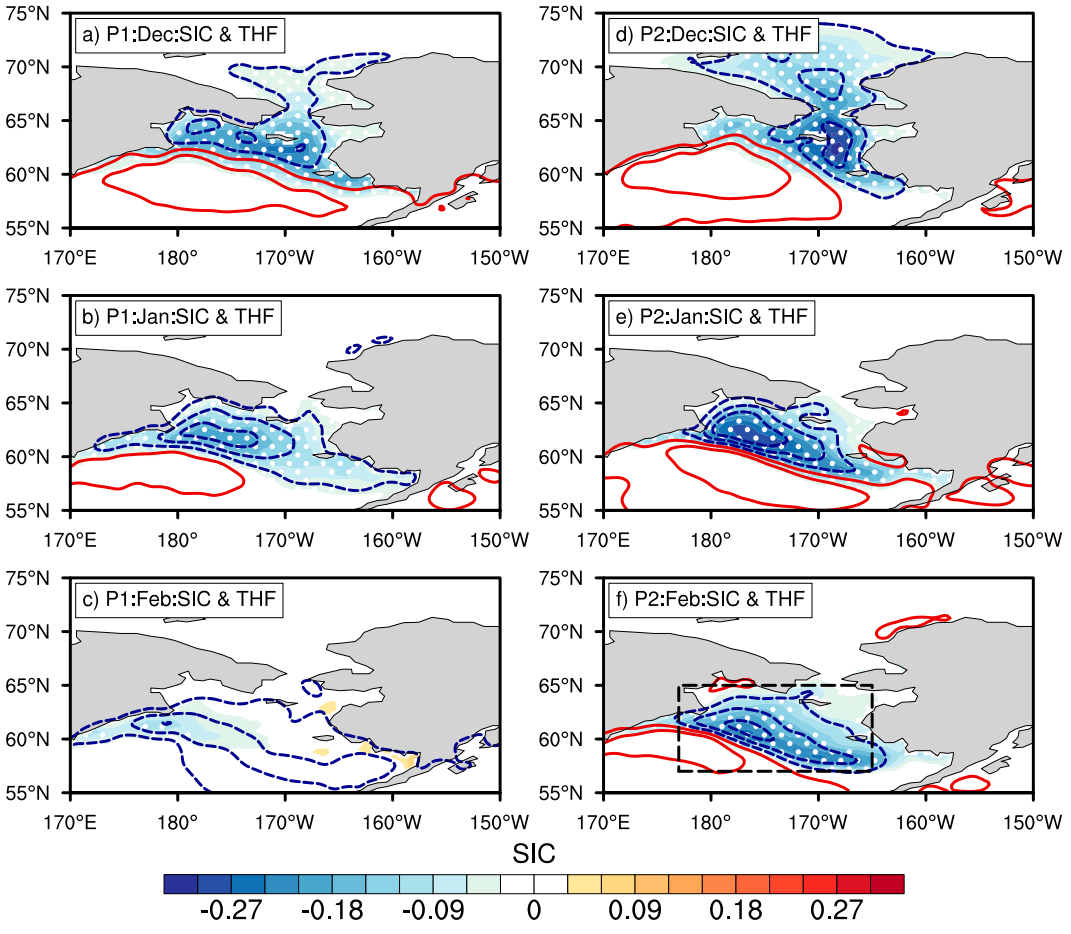

FIG. 6. Regressions of SIC (shading) and surface THF (contours) in (a),(d) December, (b),(e) January, and (c),(f) February with respect to the December SICBSI during (left) P1 and (right) P2. Red solid (blue dashed) contours indicate positive (negative) THF anomalies; note that a negative anomaly indicates upward. Dotted areas indicate that the shading values are significant at the 95% confidence level. The black dashed rectangle in (f) marks the region used to define the Feb-SICBSI.

Bering Sea ice in February, a significantly anomalous high pressure is located over the high latitudes of North Pacific region, together with significant low pressure anomaly and high pressure anomaly downstream which are located over the northern part and southern part of North America, respectively (Fig. 7a; shading). The associated horizontal WAFs indicate an apparent eastward-propagating Rossby wave train propagating from the Bering Sea to North America (Fig. 7a; vectors). It is noteworthy that the large-scale atmospheric circulation pattern associated with the Feb-SICBSI shown in Fig. 7a resembles well the one that is associated with the December SICBSI shown in Fig. 5d. This implies that the aforementioned February negative SAT anomalies over North America, which are associated with negative Bering Sea ice anomalies in the preceding December, may be a result of the February SIC anomalies that persist from the preceding December. This conclusion can be further supported by the results shown in Fig. 7b. After the linear influence of February Bering Sea ice has been removed prior to the regression analysis, the areas with significant regression coefficients of February GPH500 during P2 upon the December SICBSI (Fig. 7b) become much less compared to the results shown in Fig. 5b. Compared to the results shown in Fig. 5b, the magnitude of the horizontal WAFs shown in Fig. 7b (vectors) is much smaller, indicating a weaker eastward propagation of the planetary waves without the persistence of December Bering Sea ice anomalies.

In summary, in this section, we reveal that the December Bering Sea ice and the subsequent February SAT over North America may be physically connected during P2. The underlying physical mechanism can be summarized as follows. The negative Bering Sea ice anomalies in December persist well into the following February during which the Bering Sea ice anomalies warm the atmosphere aloft through an increase in the surface upward THF in situ. The thermal anomalies induce a Rossby wave train propagating from the Bering Sea to North America, which leads to a significant meridional dipole pattern in the atmospheric circulation over North America. Such a meridional dipole pattern promotes the colder air intrusion over the central and eastern part of North America and thus leads to significantly negative SAT anomalies.

Brought to you by UNIVERSITETSBIBLIOTEKET I | Unauthenticated | Downloaded 04/25/23 11:32 AM UTC

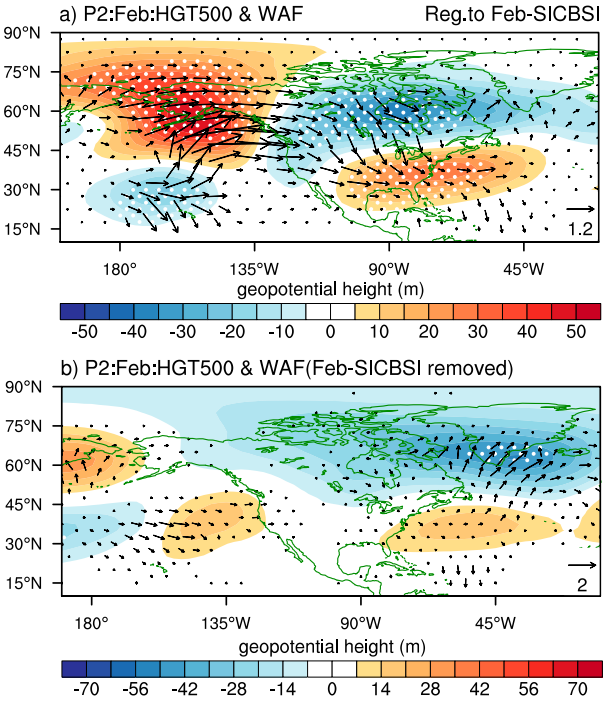

FIG. 7. (a) Regressions of February GPH500 (shading) with respect to the Feb-SICBSI during P2 with the corresponding horizontal WAFs (vectors). (b) As in Fig. 5d, but the linear influence of the Feb-SICBSI has been removed prior to the regression analysis. Dotted areas in each panel indicate that the shading values are significant at the 95% confidence level.

During P1, however, the situation is much different. The December SIC anomalies in the Bering Sea exhibits a weaker persistence (e.g., there are almost no significant SIC anomalies in the following February in the Bering Sea), thereby having weaker impacts on the subsequent February SAT over North America. The results indicate that the interdecadal change of the persistence of December Bering Sea ice anomaly around 2000 may be responsible for the strengthening of the sea ice–SAT linkage identified in this study.

5. Discussion on longer persistence of December Bering Sea ice anomaly

The analysis in section 4 reveals that the December Bering Sea ice anomaly has longer persistence in P2 than in P1. The underlying physical mechanism will be further investigated in this section. Previous studies have revealed an important atmosphere–ocean–ice interaction in the wintertime Arctic climate system, which might play a central role in the multidecadal climate changes over Arctic regions (Dai et al. 2019; Deng and Dai 2022). Through changing the energy exchange between the ocean and the atmosphere aloft, SIC variations can cause a collaborative change in both the oceanic and the atmospheric conditions (e.g., SSTs, SAT, etc.) via the atmosphere–ocean–ice coupling. As suggested by Deng and Dai (2022), sea ice reductions induced by higher SSTs in winter can cause an increase in the surface upward longwave radiation and the surface upward energy flux, which can warm the frigid air aloft. The resultant warmer air will in turn increase the surface downward longwave radiation, and further melt sea ice or prevent sea ice growth. These processes indicate a positive feedback loop that amplifies the SST-induced sea ice reductions. The intensity of such positive feedback can therefore affect the persistence of the SST-induced SIC anomaly; stronger feedback favors longer persistence of the SIC anomaly. From this perspective, we next investigate the difference of the intensity of the atmosphere–ocean–ice interaction in the Bering Sea between the two subperiods. The difference is investigated from two distinct aspects: 1) the climatological background and 2) the anomalies associated with SIC variations. As shown in Fig. 8, monthly mean SIC in the north of the Being Sea region (i.e., 60°–65°N, 160°W–180°) has significantly smaller climatology during P2 than during P1 in December (Figs. 8a–c; shading), January (Figs. 8d–f; shading), and February (Figs. 8g–i; shading) (also see Fig. 9a). Meanwhile, there are more open-water areas in the Bering Sea in December–February during P2 than during P1 (Fig. 9b). Less SIC and more open water allows the warm ocean to release more heat to warm the atmosphere aloft, thereby leading to a significant increase in the climatology of the surface upward longwave radiation in December–February from P1 to P2 (Fig. 9c). This demonstrates that Bering Sea ice variations in December–February have a stronger thermal effect on the atmosphere aloft during P2 than during P1. The more heat released from the ocean in the Bering Strait to the air aloft in P2 leads to higher air temperatures, and the warmer air in turn releases more heat to warm the ocean, which is reflected by an increase in the climatology of the SAT (Fig. 9d) and the surface downward longwave radiation (Fig. 9e) in December–February from P1 to P2. The comparison of the heat exchange between the ocean in the Bering Strait and the air aloft during the two subperiods indicates that the atmosphere–ocean–ice interaction is stronger in December–February during P2 than during P1.

To confirm if the aforementioned changes of the climatological conditions in the Bering Sea during P2 can provide more favorable climatological background for longer persistence of the SIC anomalies from December to the following February, we next compare the persistence of interannual anomalies of the longwave radiation and temperature that is related to the interannual variability of December Bering Sea ice between the two subperiods. In December during each period, the negative SIC anomaly in the Bering Sea allows the ocean to warm more the atmosphere aloft through a significant increase in the surface upward longwave radiation (Figs. 10a,d). This leads to significantly positive SAT anomalies around the Bering Strait (Figs. 11a,d). The warmer air in turn warms more the ocean/sea ice through a significant increase in the surface downward longwave radiation (Figs. 12a,d), which may partly offset the seasonal cooling (and sea ice growth) from December to January and help maintain the December negative SIC anomaly. Similar processes occur in the subsequent months (i.e., January and February) (panels b, c, e, f in Figs. 10–12), but obvious differences appear between the two subperiods. Due to the different background between the two subperiods (e.g.,

Brought to you by UNIVERSITETSBIBLIOTEKET I | Unauthenticated | Downloaded 04/25/23 11:32 AM UTC

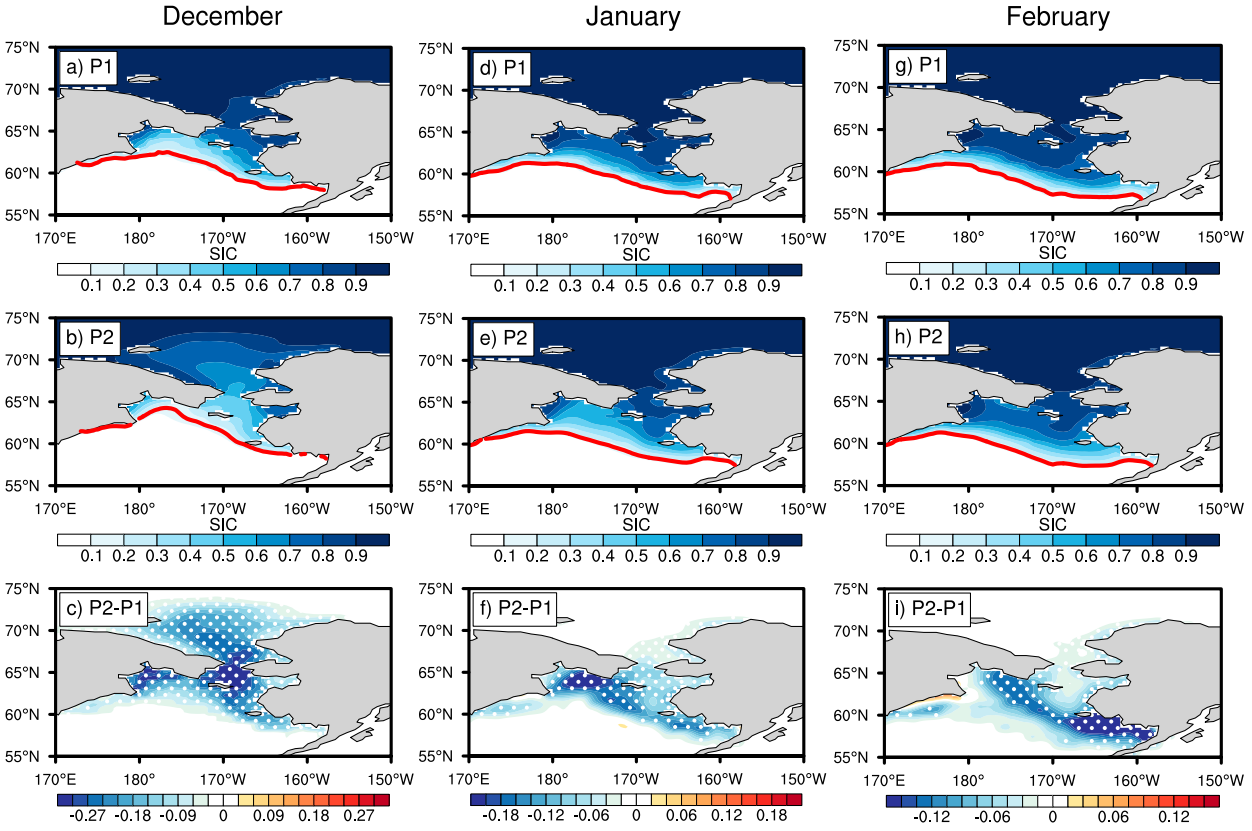

FIG. 8. Climatology of December SIC during (a) P1 and (b) P2, and (c) their differences (latter minus former). (d)–(f) As in (a)–(c), but for January SIC. (g)–(i) As in (a)–(c), but for February SIC. Red contours in the top and middle rows represent the ice edge that is represented by a SIC value of 0.15. Dotted areas in the bottom row indicate that the values are significant at the 90% confidence level. Note that the data in this figure have not been detrended so as to discuss the difference of the climatological background between P1 and P2.

more open water and stronger atmosphere–ocean–ice interaction in the Bering Sea during P2; Figs. 8 and 9), the interannual anomalies of longwave radiation and temperature related to the December SIC variations in the Bering Sea have longer persistence during P2. For example, the anomalies of the surface upward longwave radiation in January and February during P2 are wider and more significant than those in P1 (Figs. 10b,c,e,f), thereby leading to more significantly positive anomalies of the SAT around the Bering Strait (Figs. 11b,c,e,f). Correspondingly, the warmer air in turn leads to more significant anomalies of the surface downward longwave radiation in January and February during P2 (Figs. 12b,c,e,f). The results indicate that the longer persistence of the December SIC anomaly in the Bering Sea during P2 is attributed to the stronger atmosphere–ocean–ice interaction during December–February, which is associated with such a SIC anomaly.

Note that despite the fact that the AA has led to a sharp decrease of the sea ice in the Arctic during recent decades, there is still some sea ice remaining in the Bering Sea in December–February during P2 (Figs. 8b,e,h). This is a prerequisite for the SIC anomaly in the Bering Sea to affect the atmosphere through changes of the surface fluxes, which in turn affects the persistence of the SIC anomaly. As the dramatic Arctic warming continues, there might be no winter sea ice left in the Bering Sea in the coming decades (Overland and Wang 2007; Wang et al. 2012; Sun et al. 2015). At that time, the above-mentioned processes may no longer exist, and the feedback and interaction over the Bering Sea discussed in this paper may be much different, which needs further investigation in future studies.

6. Discussion of the potential drivers of December Bering Sea ice variability

The analysis in section 4 reveals a strengthened impact of December Bering Sea ice on the subsequent February SAT over North America on the interannual time scale. A question remaining is what has caused the interannual anomaly of December Bering Sea ice. Previous studies indicate that SIC anomaly in the Bering Sea can be induced by changes in both the local atmospheric and oceanic conditions, such as the winds (Sasaki and Minobe 2005), the storms (Overland and Pease 1982), the ice influx (Zhang et al. 2010), and the SST (Nakanowatari et al. 2015). Associated with reduced December SIC in the Bering Sea, there are significantly negative THF anomalies over the Bering Sea in December (Figs. 6a,d; contours). Such an in-phase relationship between the anomaly

Brought to you by UNIVERSITETSBIBLIOTEKET I | Unauthenticated | Downloaded 04/25/23 11:32 AM UTC

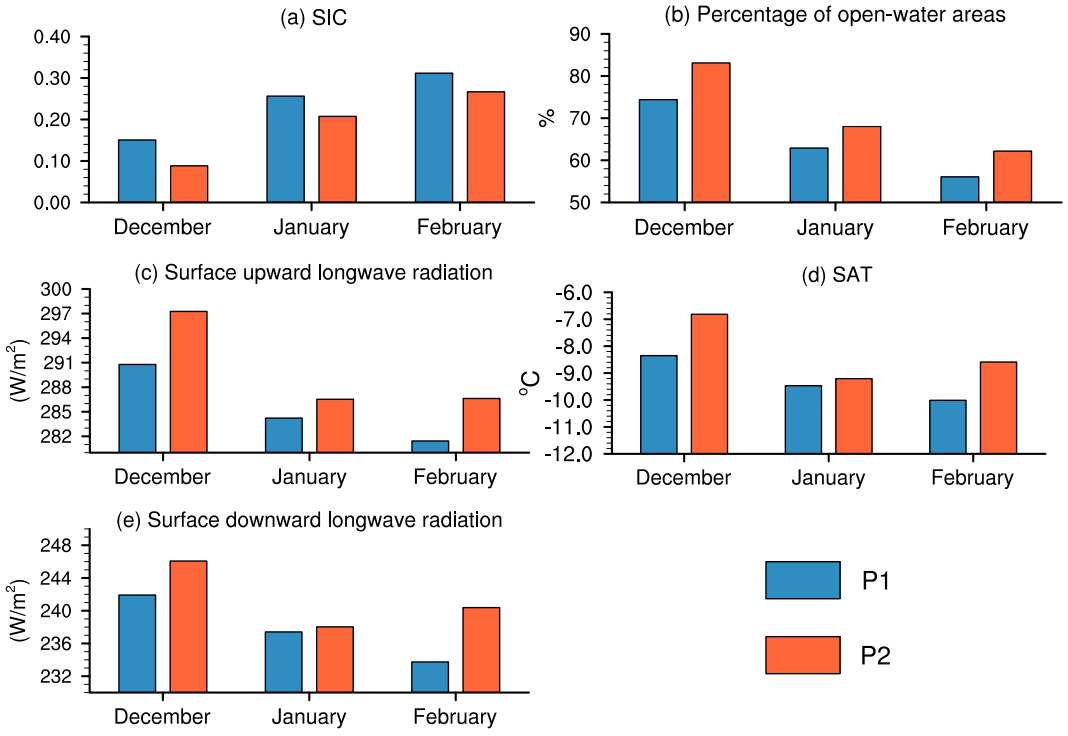

FIG. 9. Climatological conditions in the Bering Sea (55°–65°N, 165°E–155°W) during P1 (blue bars) and P2 (orange bars) from December to February for the area-averaged (a) SIC, (b) percentage of open-water areas (where SIC is less than 0.15), (c) surface upward longwave radiation, (d) SAT, and (e) surface downward longwave radiation. Note that the data in this figure have not been detrended.

of the SIC and the THF indicates that the Bering Sea ice anomalies in December drive the atmospheric variability aloft (see section 4). In other words, the Bering Sea ice anomalies in December are not likely to be caused by the simultaneous atmospheric circulation anomalies; instead, they are likely to be induced by the simultaneous or preceding oceanic anomalies (e.g., SIC, SST, etc.).

In November, since most areas in the Bering Sea are free of sea ice (Fig. 2a; red contours), there are almost no significant SIC anomalies in the Pacific sectors (Figs. 13a,e) preceding the significantly negative SIC anomalies in December (Figs. 6a,d; shading). It suggests clearly that the December SIC anomalies in the Bering Sea are likely to be induced by the simultaneous and/or preceding SST anomalies. It is found that there are significantly positive SST anomalies in the Bering Sea in December that directly cause these negative SIC anomalies (Figs. 13b,f). Interestingly, a similar SST anomaly field also emerges in November (Figs. 13c,g; shading), which is concurrent with significantly positive THF anomalies in situ (Figs. 13c,g; contours). Note that an in-phase relationship between the anomaly of the SST and the THF (positive THF anomaly indicates downward) implies that the atmosphere drives the SST anomaly while an out-of-phase relationship indicates the driving effects of the SST anomaly on the atmosphere. Therefore, the in-phase relationship between the anomaly of the SST and the THF shown in Figs. 13c and 13g indicates that the Bering Sea SST anomalies in November are driven by the simultaneous atmospheric anomalies. In October, there are almost no significant SST anomalies preceding the negative Bering Sea ice anomalies in December (Figs. 13d,h). This indicates that the Bering Sea ice anomalies in December are attributed mainly to the November SST anomalies.

Therefore, from the perspective of the atmospheric anomaly, we further explore the potential drivers that lead to November SST anomalies in the Bering Sea. Figures 14a and 14b illustrate the regressions of November GPH500 (shading) upon the December SICBSI in the two subperiods with the corresponding horizontal WAFs (vectors). Preceding reduced December SIC in the Bering Sea, a significantly anomalous high pressure is located over the high latitudes of North Pacific region in November (Figs. 14a,b; shading). This atmospheric pattern leads to positive SST anomalies in the Bering Sea through inducing an increase in the surface downward THF (Figs. 13c,g; contours). Note that apart from the high pressure, there is also an anomalous low pressure downstream over North America (Figs. 14a,b; shading). This low pressure anomaly is concurrent with significant above-normal snow cover in the central North America (around 40°–60°N; Figs. 14c,d). Previous studies indicate that variations in snow conditions can affect the atmosphere aloft via radiative and thermodynamical effects (Cohen and Rind 1991; Ellis and Leathers 1998; Henderson et al. 2018; Ye and Wu 2017). On the other hand, atmospheric variability can also lead to variations in the snow conditions (Zhang et al. 2021). Therefore, a question emerges:

Brought to you by UNIVERSITETSBIBLIOTEKET I | Unauthenticated | Downloaded 04/25/23 11:32 AM UTC

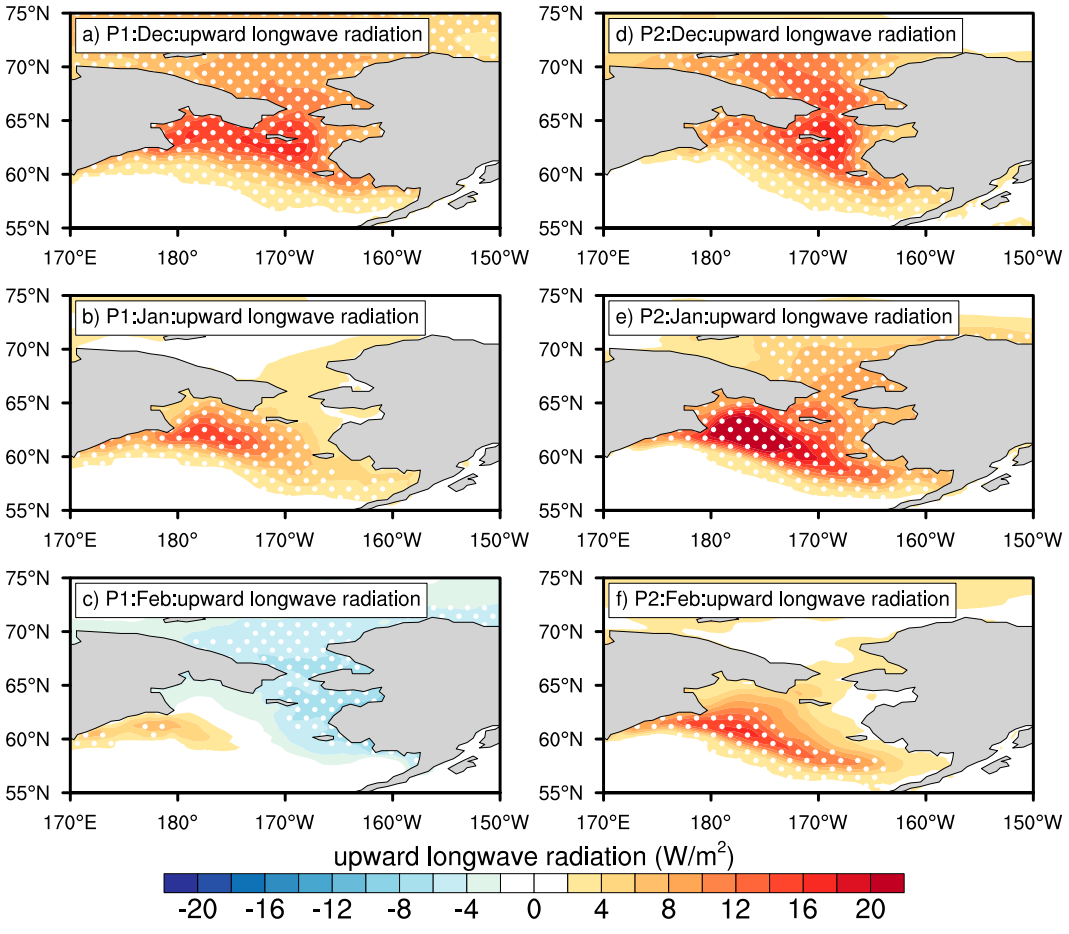

FIG. 10. Regressions of (a) December, (b) January, and (c) February surface upward longwave radiation with respect to the December SICBSI during P1. (d)–(f) As in (a)–(c), but during P2. Dotted areas indicate that the values are significant at the 95% confidence level. Positive anomalies indicate that the surface upward longwave radiation is stronger than normal.

whether the November snow cover anomalies in North America are caused by the atmospheric anomalies aloft or inversely they drive the atmospheric anomalies. We can address it by analyzing changes in the land–air heat exchange associated with the snow cover anomalies. In theory, more snow cover would increase the surface albedo, and drop land temperature by reducing the amount of solar radiation absorbed by the land surface. Therefore, if a positive anomaly of snow cover drives the atmospheric variability aloft, it would be concurrent with a positive anomaly of the surface SHF (positive SHF anomaly indicates downward). As shown in Figs. 14e and 14f, negative anomalies of surface SHF appear in the region occupied by positive snow cover anomalies, thereby indicating that the November snow cover anomalies preceding the December Bering Sea ice anomalies are induced by the atmospheric anomalies aloft.

The above results demonstrate that the November anomalies of boundary conditions such as the SST in the Bering Sea and the snow cover in North America that emerge before the reduced December SIC in the Bering Sea are driven by the November atmospheric variability. This suggests that the large-scale atmospheric circulation anomaly patterns shown in Figs. 14a and 14b may be attributed to internal variability that originates from the atmospheric dynamics instead of the ocean or the land. The associated horizontal WAFs indicates an apparent eastward-propagating Rossby wave train propagating from the subtropical western North Pacific to North America (Figs. 14a,b; vectors). This pattern is similar to the positive phase of the EP-NP teleconnection pattern. The correlation coefficients between the December SICBSI and the November EP-NP index are 0.40 (significant at 95% confidence level) during P1 and 0.40 (significant at 90% confidence level) during P2. The results show that the large-scale atmospheric circulation anomalies in November leads to the simultaneously anomalies of the SST in the Bering Sea and the snow cover in North America. The November SST anomalies in the Bering Sea could well persist into the following December, leading to significant SIC anomalies.

7. Conclusions

This study identifies a strengthened linkage between December Bering Sea ice and subsequent February SAT over North

Brought to you by UNIVERSITETSBIBLIOTEKET I | Unauthenticated | Downloaded 04/25/23 11:32 AM UTC

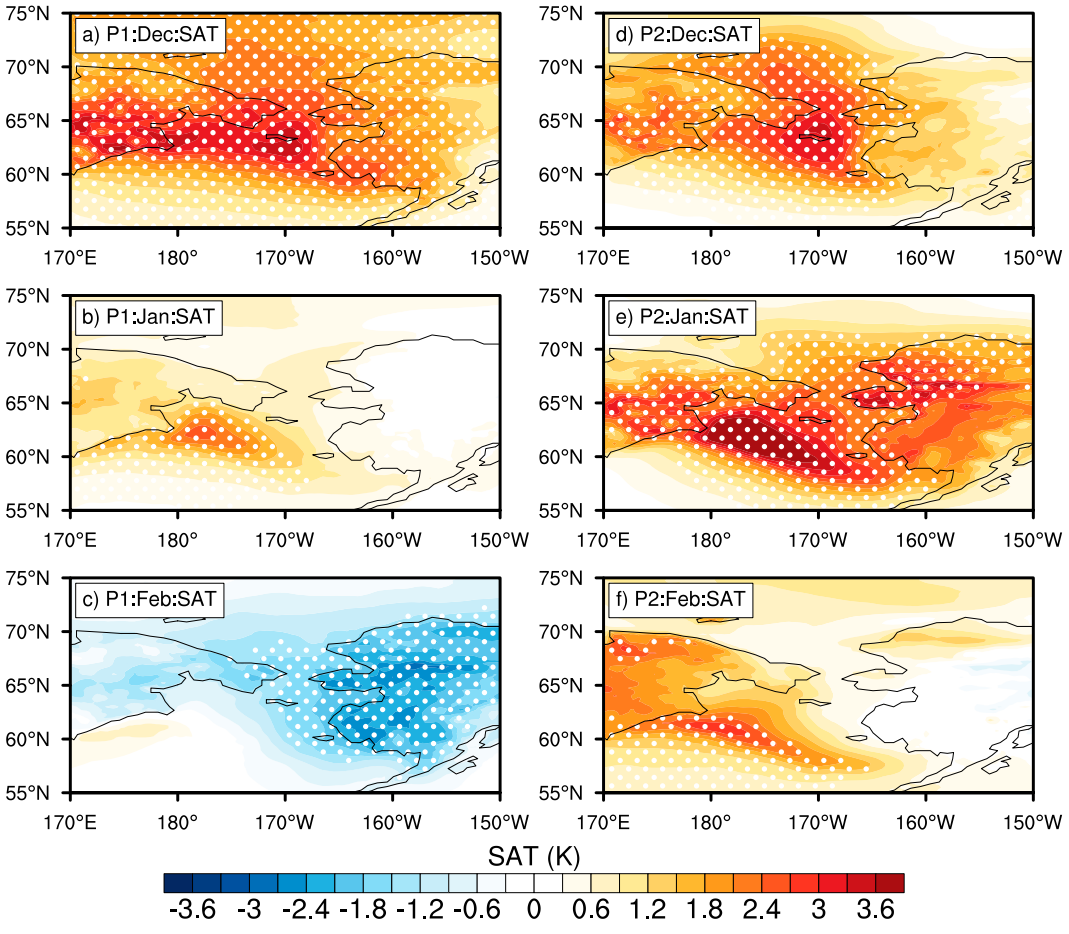

FIG. 11. Regressions of (a) December, (b) January, and (c) February SAT with respect to the December SICBSI during P1. (d)–(f) As in (a)–(c), but during P2. Dotted areas indicate that the values are significant at the 95% confidence level.

America after the late 1990s. Our analysis shows that reduced December SIC in the Bering Sea is followed by significantly negative SAT anomalies over North America (mainly in the central and eastern part) in the following February during P2 (Fig. 5b), which is not the case during P1 (Fig. 5a). During P2, it is found that reduced December SIC in the Bering Sea is generally associated with an anomalous meridional dipole pattern in the atmospheric circulation over North America in the subsequent February (Fig. 5d). The resultantly anomalous northerlies at 850 hPa reflect more intense cold air outbreaks, resulting in significantly colder temperatures in the central and eastern part of North America. By contrast, this situation is barely observed during P1 (Fig. 5c). Further work indicates that the December Bering Sea ice and the subsequent February SAT over North America may be physically connected during P2 due to the intrinsic persistence of the SIC anomaly in the Bering Sea, and the strengthened sea ice–SAT linkage can be attributed to the longer persistence of the SIC anomaly during P2. During P2, the significantly negative SIC anomaly in the northern part of the Bering Sea can persist well from December into the following February (Figs. 6d–f). The analysis of the simultaneous relationship between the anomaly of the SIC and the surface THF in situ in February reveals that the SIC anomaly in February plays a predominant role in the atmosphere–ocean–ice interaction in the Bering Sea. That is, a significant SIC anomaly in February can lead to warming in the air aloft, and also cause a significantly anomalous high pressure over the high latitudes of North Pacific region (Fig. 7a). Such a causal effect of the negative SIC anomaly is indicated by 1) the anomalous surface upward THF (Fig. 6f; contours) and 2) an eastward-propagating Rossby wave train originating from the Bering Sea (Fig. 7a). By contrast, during P1, the December SIC anomaly in the Bering Sea cannot persist into the subsequent February (Figs. 6a–c).

We next investigate the physical mechanism underlying the longer persistence of December SIC anomaly in the Bering Sea during P2. Previous studies have emphasized the importance of atmosphere–ocean–ice interaction in explaining the wintertime anomalies in the Arctic climate system (Dai et al. 2019; Deng and Dai 2022). That is, sea ice decline in winter allows the warm ocean to release more heat to warm the frigid air aloft, and the resultant warmer air will in turn increase the downward heat transport, which further amplifies the sea ice decline. This process indicates a positive feedback loop,

Brought to you by UNIVERSITETSBIBLIOTEKET I | Unauthenticated | Downloaded 04/25/23 11:32 AM UTC

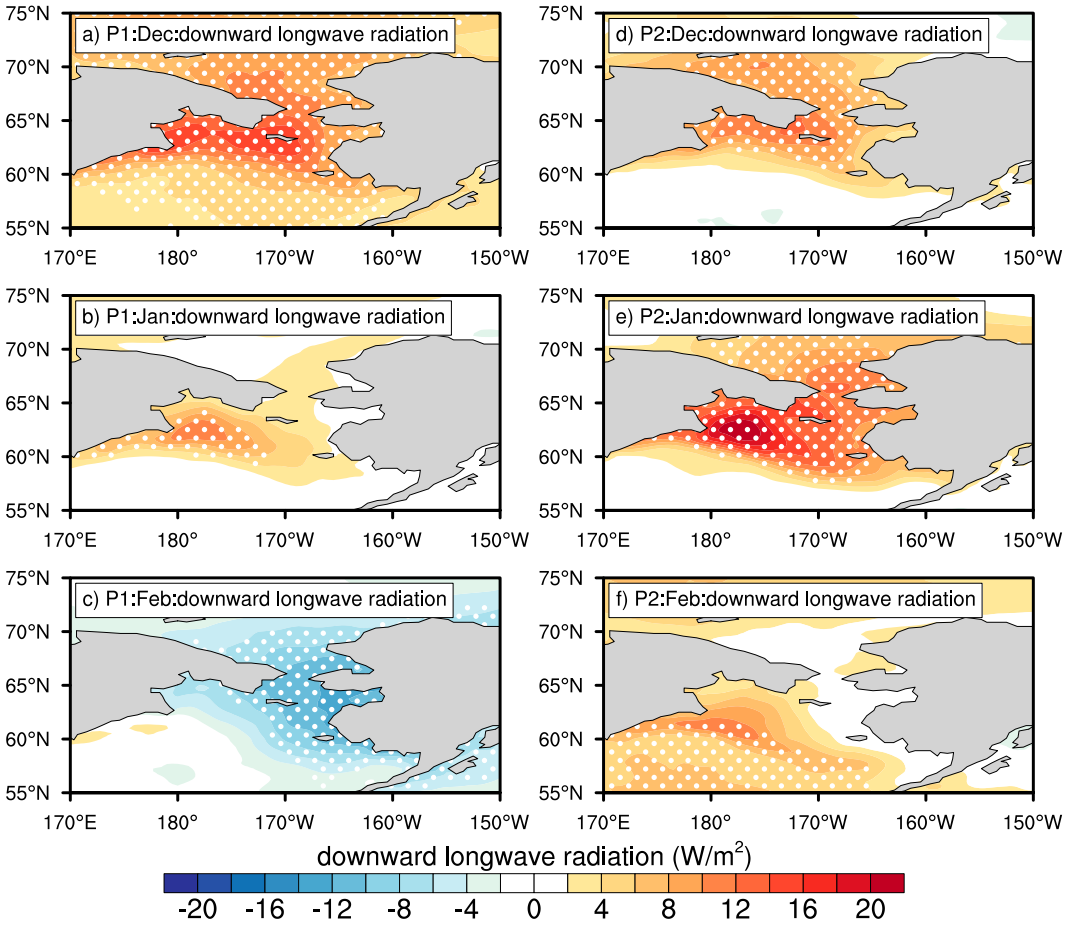

FIG. 12. Regressions of (a) December, (b) January, and (c) February surface downward longwave radiation with respect to the December SICBSI during P1. (d)–(f) As in (a)–(c), but during P2. Dotted areas indicate that the values are significant at the 95% confidence level. Positive anomalies indicate that the surface downward longwave radiation is stronger than normal.

which is favorable for the persistence of the SIC anomaly. Therefore, we then compare the intensity of the atmosphere–ocean–ice interaction in the Bering Sea between P1 and P2. The surface upward longwave radiation (which can reflect the effects of warmer SST related to sea ice reduction) and surface downward longwave radiation (which can reflect the effects of warmer air aloft) are taken into account to characterize the intensity of the atmosphere–ocean–ice interaction. Stronger atmosphere–ocean–ice interaction demonstrates that there are increased heat and energy exchanges between the ocean and the air aloft, corresponding to an increase in both the surface upward longwave radiation and surface downward longwave radiation. Comparison of the climatological conditions in the Bering Sea between P1 and P2 indicates that there are less climatological sea ice and more open water in the Bering Sea from December to the following February during P2 (Figs. 8 and 9a,b), which leads to an increase in the climatology of the surface upward longwave radiation, the SAT, and the surface downward longwave radiation in December–February from P1 to P2 (Figs. 9c–e). The clearly indicates that the Bering Sea atmosphere–ocean–ice interaction from December to the following February in P2 is stronger than that in P1, which provides more favorable climatological background for the longer persistence of the December SIC anomaly. In December, associated with reduced December SIC in the Bering Sea, significantly positive anomalies of the surface upward longwave radiation (Figs. 10a,d), the SAT (Figs. 11a,d), and the surface downward longwave radiation (Figs. 12a,d) appear over the Bering Strait during each period, which reflects the aforementioned positive feedback loop within the atmosphere–ocean–ice interaction. In January and February, these anomalies of longwave radiations and temperature are wider and more significant in P2 than in P1 (Figs. 10b,c,e,f, 11b,c,e,f, 12b,c,e,f). This shows that the positive feedback loop related to the SIC anomaly within the atmosphere–ocean–ice interaction during P2 is stronger than that during P1, which leads to the longer persistence of the December SIC anomaly in the Bering Sea.

We further investigate the potential drivers of the interannual anomaly of December SIC in the Bering Sea. Our

Brought to you by UNIVERSITETSBIBLIOTEKET I | Unauthenticated | Downloaded 04/25/23 11:32 AM UTC

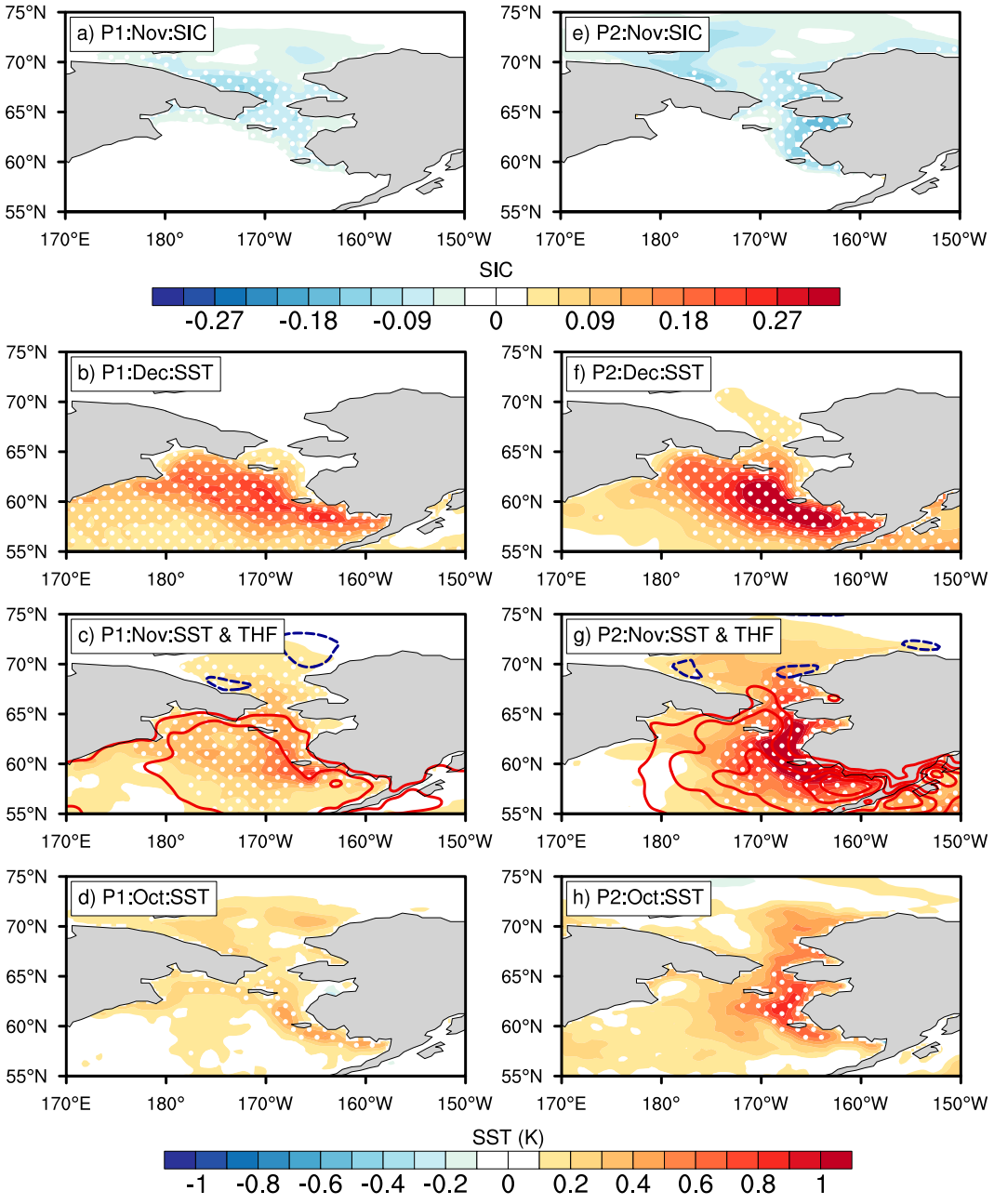

FIG. 13. Regressions of (a) November SIC, (b) December SST, (c) November SST, and (d) October SST with respect to the December SICBSI during P1 (shading). Contours in (c) show the regressions of November surface THF with respect to the December SICBSI during P1. Red solid (blue dashed) contours indicate positive (negative) THF anomaly; note that a positive anomaly indicates downward. (e)–(h) As in (a)–(d), but during P2. Dotted areas in each panel indicate that the shading values are significant at the 95% confidence level.

analysis demonstrates that there is an in-phase relationship between the anomaly of the December SIC in the Bering Sea and the surface THF in situ (Figs. 6a,d), indicating that the SIC anomaly drives the atmospheric variability aloft. This indicates that the SIC anomaly in December is likely to be induced by the simultaneous or preceding oceanic anomalies (e.g., SIC, SST, etc.), instead of the simultaneous atmospheric circulation anomalies. Further analysis indicates that the negative anomaly of December SIC in the Bering Sea is a result of the persistence of a positive SST anomaly in the preceding November (Figs. 13c,g; shading), which is induced by the simultaneous atmospheric circulation anomalies aloft through an increase in the surface downward THF (Figs. 13c,g; contours). It is found that the November large-scale atmospheric

Brought to you by UNIVERSITETSBIBLIOTEKET I | Unauthenticated | Downloaded 04/25/23 11:32 AM UTC

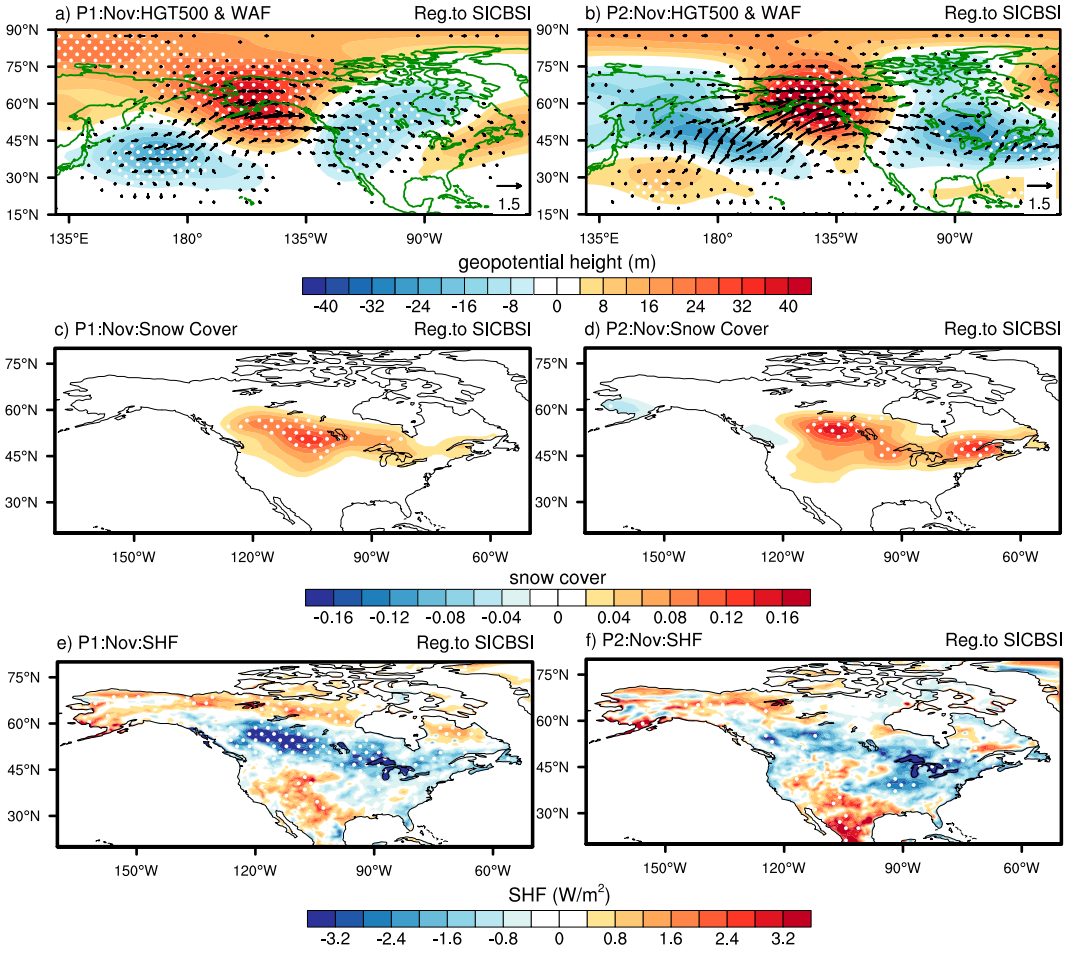

FIG. 14. Regressions of November (a) GPH500 (shading), (c) snow cover, and (e) surface SHF (negative anomaly indicates upward) with respect to the December SICBSI during P1. Vectors in (a) show the associated horizontal WAFs. (b),(d),(f) As in (a), (c), and (e), but during P2. Dotted areas in each panel indicate that the shading values are significant at the 90% confidence level.

circulation anomalies simultaneously lead to such a positive SST anomaly in the Bering Sea together with some other anomalies of boundary conditions, such as a positive snow cover anomaly in North America through an increase in the surface upward SHF (Figs. 14c–f). This suggests that the November large-scale atmospheric circulation anomalies, which are found to be similar to the positive phase of the EP-NP teleconnection pattern, may be attributed to atmospheric internal variability.

Acknowledgments. This research was supported by the National Natural Science Foundation of China (Grants 42088101, 41991280, and 41875118), and the Research Council of Norway projects BASIC and MAPARC (Grants 325440 and 328943).

Data availability statement. All the data analyzed in this study are openly available. The ERA5 reanalysis data were retrieved from the data portal at https://cds.climate.copernicus.eu/#!/search?text=ERA5&type=dataset. Monthly snow cover extent was obtained from the Rutgers University GSL at http://climate.rutgers.edu/snowcover/. The EP-NP index was obtained from the NOAA CPC website at https://www.cpc.ncep.noaa.gov/data/teledoc/ep.shtml.

REFERENCES

Arrhenius, S., 1897: On the influence of carbonic acid in the air upon the temperature of the Earth. *Publ. Astron. Soc. Pac.*, **9**, 14, https://doi.org/10.1086/121158.

Blackport, R., and J. Screen, 2020: Weakened evidence for mid-latitude impacts of Arctic warming. *Nat. Climate Change*, **10**, 1065–1066, https://doi.org/10.1038/s41558-020-00954-y.

——, and ——, 2021: Observed statistical connections overestimate the causal effects of Arctic sea ice changes on mid-latitude winter climate. *J. Climate*, **34**, 3021–3038, https://doi.org/10.1175/JCLI-D-20-0293.1.

——, ——, K. Wiel, and R. Bintanja, 2019: Minimal influence of reduced Arctic sea ice on coincident cold winters in mid-latitudes.

Brought to you by UNIVERSITETSBIBLIOTEKET I | Unauthenticated | Downloaded 04/25/23 11:32 AM UTC

Nat. Climate Change, **9**, 697–704, https://doi.org/10.1038/s41558-019-0551-4.

——, J. Fyfe, and J. Screen, 2022: Arctic change reduces risk of cold extremes. *Science*, **375**, 729, https://doi.org/10.1126/science.abn2414.

Bretherton, C. S., M. Widmann, V. P. Dymnikov, J. M. Wallace, and I. Bladé, 1999: The effective number of spatial degrees of freedom of a time-varying field. *J. Climate*, **12**, 1990–2009, https://doi.org/10.1175/1520-0442(1999)012<1990:TENOSD>2.0.CO;2.

Chen, X., and D. Luo, 2017: Arctic sea ice decline and continental cold anomalies: Upstream and downstream effects of Greenland blocking. *Geophys. Res. Lett.*, **44**, 3411–3419, https://doi.org/10.1002/2016GL072387.

Chen, Z., S.-R. Zhang, A. J. Coster, and G. Fang, 2015: EOF analysis and modeling of GPS TEC climatology over North America. *J. Geophys. Res. Space Phys.*, **120**, 3118–3129, https://doi.org/10.1002/2014JA020837.

Cohen, J., and D. Rind, 1991: The effect of snow cover on the climate. *J. Climate*, **4**, 689–706, https://doi.org/10.1175/1520-0442(1991)004<0689:TEOSCO>2.0.CO;2.

——, J. C. Furtado, M. Barlow, V. A. Alexeev, and J. E. Cherry, 2012: Asymmetric seasonal temperature trends. *Geophys. Res. Lett.*, **39**, L04705, https://doi.org/10.1029/2011GL050582.

——, and Coauthors, 2014: Recent Arctic amplification and extreme mid-latitude weather. *Nat. Geosci.*, **7**, 627–637, https://doi.org/10.1038/ngeo2234.

——, K. Pfeiffer, and J. A. Francis, 2018: Warm Arctic episodes linked with increased frequency of extreme winter weather in the United States. *Nat. Commun.*, **9**, 869, https://doi.org/10.1038/s41467-018-02992-9.

——, and Coauthors, 2020: Divergent consensuses on Arctic amplification influence on midlatitude severe winter weather. *Nat. Climate Change*, **10**, 20–29, https://doi.org/10.1038/s41558-019-0662-y.

——, L. Agel, M. Barlow, C. I. Garfinkel, and I. White, 2021: Linking Arctic variability and change with extreme winter weather in the United States. *Science*, **373**, 1116–1121, https://doi.org/10.1126/science.abi9167.

Dai, A., and M. Song, 2020: Little influence of Arctic amplification on mid-latitude climate. *Nat. Climate Change*, **10**, 231–237, https://doi.org/10.1038/s41558-020-0694-3.

——, and J. Deng, 2022: Recent Eurasian winter cooling partly caused by internal multidecadal variability amplified by Arctic sea ice–air interactions. *Climate Dyn.*, **58**, 3261–3277, https://doi.org/10.1007/s00382-021-06095-y.

——, D. Luo, M. Song, and J. Liu, 2019: Arctic amplification is caused by sea-ice loss under increasing CO_2. *Nat. Commun.*, **10**, 121, https://doi.org/10.1038/s41467-018-07954-9.

Deng, J., and A. Dai, 2022: Sea ice–air interactions amplify multidecadal variability in the North Atlantic and Arctic region. *Nat. Commun.*, **13**, 2100, https://doi.org/10.1038/s41467-022-29810-7.

Deser, C., R. Tomas, M. Alexander, and D. Lawrence, 2010: The seasonal atmospheric response to projected Arctic sea ice loss in the late twenty-first century. *J. Climate*, **23**, 333–351, https://doi.org/10.1175/2009JCLI3053.1.

Ellis, A. W., and D. J. Leathers, 1998: The effects of a discontinuous snow cover on lower atmospheric temperature and energy flux patterns. *Geophys. Res. Lett.*, **25**, 2161–2164, https://doi.org/10.1029/98GL01582.

Estilow, T. W., A. H. Young, and D. A. Robinson, 2015: A long-term Northern Hemisphere snow cover extent data record for climate studies and monitoring. *Earth Syst. Sci. Data*, **7**, 137–142, https://doi.org/10.5194/essd-7-137-2015.

Fischer, E. M., and R. Knutti, 2014: Heated debate on cold weather. *Nat. Climate Change*, **4**, 537–538, https://doi.org/10.1038/nclimate2286.

Francis, J. A., 2017: Why are Arctic linkages to extreme weather still up in the air? *Bull. Amer. Meteor. Soc.*, **98**, 2551–2557, https://doi.org/10.1175/BAMS-D-17-0006.1.

——, and S. J. Vavrus, 2012: Evidence linking Arctic amplification to extreme weather in mid-latitudes. *Geophys. Res. Lett.*, **39**, L06801, https://doi.org/10.1029/2012GL051000.

——, and ——, 2015: Evidence for a Wavier jet stream in response to rapid Arctic warming. *Environ. Res. Lett.*, **10**, 014005, https://doi.org/10.1088/1748-9326/10/1/014005.

——, N. Skific, and S. J. Vavrus, 2018: North American weather regimes are becoming more persistent: Is Arctic amplification a factor? *Geophys. Res. Lett.*, **45**, 112414–112422, https://doi.org/10.1029/2018GL080252.

Hanna, E., R. J. Hall, T. E. Cropper, T. J. Ballinger, L. Wake, T. Mote, and J. Cappelen, 2018: Greenland blocking index daily series 1851–2015: Analysis of changes in extremes and links with North Atlantic and UK climate variability and change. *Int. J. Climatol.*, **38**, 3546–3564, https://doi.org/10.1002/joc.5516.

Henderson, G. R., Y. Peings, J. C. Furtado, and P. J. Kushner, 2018: Snow–atmosphere coupling in the Northern Hemisphere. *Nat. Climate Change*, **8**, 954–963, https://doi.org/10.1038/s41558-018-0295-6.

Hersbach, H., and Coauthors, 2020: The ERA5 global reanalysis. *Quart. J. Roy. Meteor. Soc.*, **146**, 1999–2049, https://doi.org/10.1002/qj.3803.

Iida, M., S. Sugimoto, and T. Suga, 2020: Severe cold winter in North America linked to Bering Sea ice loss. *J. Climate*, **33**, 8069–8085, https://doi.org/10.1175/JCLI-D-19-0994.1.

Johnson, N. C., S. P. Xie, Y. Kosaka, and X. Li, 2018: Increasing occurrence of cold and warm extremes during the recent global warming slowdown. *Nat. Commun.*, **9**, 1724, https://doi.org/10.1038/s41467-018-04040-y.

Kug, J.-S., J.-H. Jeong, Y.-S. Jang, B.-M. Kim, C. K. Folland, S.-K. Min, and S.-W. Son, 2015: Two distinct influences of Arctic warming on cold winters over North America and East Asia. *Nat. Geosci.*, **8**, 759–762, https://doi.org/10.1038/ngeo2517.

Lee, M.-Y., C.-C. Hong, and H.-H. Hsu, 2015: Compounding effects of warm sea surface temperature and reduced sea ice on the extreme circulation over the extratropical North Pacific and North America during the 2013–2014 boreal winter. *Geophys. Res. Lett.*, **42**, 1612–1618, https://doi.org/10.1002/2014GL062956.

Li, C., B. Stevens, and J. Marotzke, 2015: Eurasian winter cooling in the warming hiatus of 1998–2012. *Geophys. Res. Lett.*, **42**, 8131–8139, https://doi.org/10.1002/2015GL065327.

Li, H., S. He, K. Fan, Y. Liu, and X. Yuan, 2021: Recent intensified influence of the winter North Pacific sea surface temperature on the mei-yu withdrawal date. *J. Climate*, **34**, 3869–3887, https://doi.org/10.1175/JCLI-D-19-0768.1.

Liu, J., J. A. Curry, H. Wang, M. Song, and R. M. Horton, 2012: Impact of declining Arctic sea ice on winter snowfall. *Proc. Natl. Acad. Sci. USA*, **109**, 4074–4079, https://doi.org/10.1073/pnas.1114910109.

Liu, Y., and S. He, 2020: Strengthened linkage between November/December North Atlantic Oscillation and subsequent January

Brought to you by UNIVERSITETSBIBLIOTEKET I | Unauthenticated | Downloaded 04/25/23 11:32 AM UTC

European precipitation after the late 1980s. *J. Climate*, **33**, 8281–8300, https://doi.org/10.1175/JCLI-D-19-0662.1.

Luo, D., Y. Chen, A. Dai, M. Mu, R. Zhang, and S. Ian, 2017: Winter Eurasian cooling linked with the Atlantic Multidecadal Oscillation. *Environ. Res. Lett.*, **12**, 125002, https://doi.org/10.1088/1748-9326/aa8de8.

Martin, J. E., 2021: Recent trends in the waviness of the Northern Hemisphere wintertime polar and subtropical jets. *J. Geophys. Res. Atmos.*, **126**, e2020JD033668, https://doi.org/10.1029/2021GL096076.

McCusker, K. E., J. C. Fyfe, and M. Sigmond, 2016: Twenty-five winters of unexpected Eurasian cooling unlikely due to Arctic sea-ice loss. *Nat. Geosci.*, **9**, 838–842, https://doi.org/10.1038/ngeo2820.

McKinnon, K. A., A. Rhines, M. P. Tingley, and P. Huybers, 2016: Long-lead predictions of eastern United States hot days from Pacific sea surface temperatures. *Nat. Geosci.*, **9**, 389–394, https://doi.org/10.1038/ngeo2687.

Mori, M., M. Watanabe, H. Shiogama, J. Inoue, and M. Kimoto, 2014: Robust Arctic sea-ice influence on the frequent Eurasian cold winters in past decades. *Nat. Geosci.*, **7**, 869–873, https://doi.org/10.1038/ngeo2277.

——, Y. Kosaka, M. Watanabe, H. Nakamura, and M. Kimoto, 2019: A reconciled estimate of the influence of Arctic sea-ice loss on recent Eurasian cooling. *Nat. Climate Change*, **9**, 123–129, https://doi.org/10.1038/s41558-018-0379-3.

Nakanowatari, T., J. Inoue, K. Sato, and T. Kikuchi, 2015: Summertime atmosphere–ocean preconditionings for the Bering Sea ice retreat and the following severe winters in North America. *Environ. Res. Lett.*, **10**, 094023, https://doi.org/10.1088/1748-9326/10/9/094023.

Orsolini, Y. J., R. Senan, F. Vitart, G. Balsamo, A. Weisheimer, and F. J. Doblas-Reyes, 2016: Influence of the Eurasian snow on the negative North Atlantic Oscillation in subseasonal forecasts of the cold winter 2009/2010. *Climate Dyn.*, **47**, 1325–1334, https://doi.org/10.1007/s00382-015-2903-8.

Overland, J. E., and C. H. Pease, 1982: Cyclone climatology of the Bering Sea and its relation to sea ice extent. *Mon. Wea. Rev.*, **110**, 5–13, https://doi.org/10.1175/1520-0493(1982)110<0005:CCOTBS>2.0.CO;2.

——, and M. Wang, 2007: Future regional Arctic sea ice declines. *Geophys. Res. Lett.*, **34**, L17705, https://doi.org/10.1029/2007GL030808.

——, J. A. Francis, R. Hall, E. Hanna, S. Kim, and T. Vihma, 2015: The melting Arctic and midlatitude weather patterns: Are they connected? *J. Climate*, **28**, 7917–7932, https://doi.org/10.1175/JCLI-D-14-00822.1.

Palmer, T., 2014: Record-breaking winters and global climate change. *Science*, **344**, 803–804, https://doi.org/10.1126/science.1255147.

Park, H., S. Lee, S. Son, S. B. Feldstein, and Y. Kosaka, 2015: The impact of poleward moisture and sensible heat flux on Arctic winter sea ice variability. *J. Climate*, **28**, 5030–5040, https://doi.org/10.1175/JCLI-D-15-0074.1.

Quiroz, R. S., 1979: Tropospheric–stratospheric interaction in the major warming event of January–February 1979. *Geophys. Res. Lett.*, **6**, 645–648, https://doi.org/10.1029/GL006i008p00645.

——, 1986: The association of stratospheric warmings with tropospheric blocking. *J. Geophys. Res.*, **91**, 5277–5285, https://doi.org/10.1029/JD091iD04p05277.

Rantanen, M., A. Y. Karpechko, A. Lipponen, K. Nordling, O. Hyvärinen, K. Ruosteenoja, T. Vihma, and A. Laaksonen, 2022: The Arctic has warmed nearly four times faster than the globe since 1979. *Commun. Earth Environ.*, **3**, 168, https://doi.org/10.1038/s43247-022-00498-3.

Robinson, D. A., T. W. Estilow, and NOAA CDR Program, 2012: NOAA Climate Data Record (CDR) of Northern Hemisphere (NH) Snow Cover Extent (SCE), version 1. NOAA National Centers for Environmental Information, accessed 6 June 2021, https://www.ncei.noaa.gov/access/metadata/landing-page/bin/iso?id=gov.noaa.ncdc:C00756.

Sasaki, Y. N., and S. Minobe, 2005: Seasonally dependent interannual variability of sea ice in the Bering Sea and its relation to atmospheric fluctuations. *J. Geophys. Res.*, **110**, C05011, https://doi.org/10.1029/2004JC002486.

Screen, J., and I. Simmonds, 2010: The central role of diminishing sea ice in recent Arctic temperature amplification. *Nature*, **464**, 1334–1337, https://doi.org/10.1038/nature09051.

——, and ——, 2014: Amplified mid-latitude planetary waves favour particular regional weather extremes. *Nat. Climate Change*, **4**, 704–709, https://doi.org/10.1038/nclimate2271.

Si, D., L. Ma, P. Wang, Y. Wang, Y. Nie, and L. Sun, 2016: Anomalous activity of Arctic Oscillation in winter 2015/2016 and its impact on temperature in China. *Meteor. Mon.*, **42**, 892–897, http://qxqk.nmc.cn/qxen/article/abstract/20160713.

Sigmond, M., and J. Fyfe, 2016: Tropical Pacific impacts on cooling North American winters. *Nat. Climate Change*, **6**, 970–974, https://doi.org/10.1038/nclimate3069.

Sun, L., C. Deser, and R. A. Tomas, 2015: Mechanisms of stratospheric and tropospheric circulation response to projected Arctic sea ice loss. *J. Climate*, **28**, 7824–7845, https://doi.org/10.1175/JCLI-D-15-0169.1.

Sun, L. T., J. Perlwitz, and M. Hoerling, 2016: What caused the recent "warm Arctic, cold continents" trend pattern in winter temperatures? *Geophys. Res. Lett.*, **43**, 5345–5352, https://doi.org/10.1002/2016GL069024.

Takaya, K., and H. Nakamura, 2001: A formulation of a phase-independent wave-activity flux for stationary and migratory quasigeostrophic eddies on a zonally varying basic flow. *J. Atmos. Sci.*, **58**, 608–627, https://doi.org/10.1175/1520-0469(2001)058<0608:AFOAPI>2.0.CO;2.

Tian, Y., Y. Gao, and D. Guo, 2021: The relationship between melt season sea ice over the Bering Sea and summer precipitation over mid-latitude East Asia. *Adv. Atmos. Sci.*, **38**, 918–930, https://doi.org/10.1007/s00376-021-0348-z.

Van Oldenborgh, G. J., R. Haarsma, H. De Vries, and M. R. Allen, 2015: Cold extremes in North America vs. mild weather in Europe: The winter of 2013–14 in the context of a warming world. *Bull. Amer. Meteor. Soc.*, **96**, 707–714, https://doi.org/10.1175/BAMS-D-14-00036.1.

Vijverberg, S., D. Coumou, 2022: The role of the Pacific Decadal Oscillation and ocean–atmosphere interactions in driving US temperature predictability. *npj Climate Atmos. Sci.*, **5**, 18, https://doi.org/10.1038/s41612-022-00237-7.

Voosen, P., 2021: Arctic ice loss not a big culprit in harsh winters. *Science*, **372**, 668–669, https://doi.org/10.1126/science.372.6543.668.

Wallace, J. M., I. M. Held, D. W. J. Thompson, K. E. Trenberth, and J. E. Walsh, 2014: Global warming and winter weather. *Science*, **343**, 729–730, https://doi.org/10.1126/science.343.6172.729.

Wang, D., T. Cui, D. Si, X. Shao, Q. Li, and C. Sun, 2015: Features and possible causes for East Asian winter monsoon in 2014/2015. *Meteor. Mon.*, **41**, 907–914, http://qxqk.nmc.cn/qxen/article/abstract/20150713.

Wang, M. Y., J. E. Overland, and P. Stabeno, 2012: Future climate of the Bering and Chukchi Seas projected by global climate

Brought to you by UNIVERSITETSBIBLIOTEKET I | Unauthenticated | Downloaded 04/25/23 11:32 AM UTC

models. *Deep-Sea Res. II*, **65–70**, 46–57, https://doi.org/10.1016/j.dsr2.2012.02.022.

Wegmann, M., Y. Orsolini, and O. Zolina, 2018: Warm Arctic–cold Siberia: Comparing the recent and the early 20th-century Arctic warmings. *Environ. Res. Lett.*, **13**, 025009, https://doi.org/10.1088/1748-9326/aaa0b7.

Xie, W., G. Fan, R. Ding, J. Li, B. Li, J. Qin, and X. Zhou, 2019: Interdecadal change in the lagged relationship between the Victoria mode and ENSO. *Atmos. Ocean. Sci. Lett.*, **12**, 294–301, https://doi.org/10.1080/16742834.2019.1620081.

Xie, Y., G. Wu, Y. Liu, J. Huang, and H. Nie, 2022: A dynamic and thermodynamic coupling view of the linkages between Eurasian cooling and Arctic warming. *Climate Dyn.*, **58**, 2725–2744, https://doi.org/10.1007/s00382-021-06029-8.

Xu, X., S. He, Y. Gao, T. Furevik, H. Wang, F. Li, and F. Ogawa, 2019: Strengthened linkage between midlatitudes and Arctic in boreal winter. *Climate Dyn.*, **53**, 3971–3983, https://doi.org/10.1007/s00382-019-04764-7.

Ye, K., and R. Wu, 2017: Autumn snow cover variability over northern Eurasia and roles of atmospheric circulation. *Adv. Atmos. Sci.*, **34**, 847–858, https://doi.org/10.1007/s00376-017-6287-z.

——, T. Jung, and T. Semmler, 2018: The influences of the Arctic troposphere on the midlatitude climate variability and the recent Eurasian cooling. *J. Geophys. Res. Atmos.*, **123**, 102162–102184, https://doi.org/10.1029/2018JD028980.

Yu, S., and J. Sun, 2021: Conditional impact of boreal autumn North Atlantic SST anomaly on winter tropospheric Asian polar vortex. *Climate Dyn.*, **56**, 855–871, https://doi.org/10.1007/s00382-020-05507-9.

Zhang, J., R. Woodgate, and R. Moritz, 2010: Sea ice response to atmospheric and oceanic forcing in the Bering Sea. *J. Phys. Oceanogr.*, **40**, 1729–1747, https://doi.org/10.1175/2010JPO4323.1.

Zhang, P., Y. Wu, G. Chen, and Y. Yu, 2020: North American cold events following sudden stratospheric warming in the presence of low Barents-Kara Sea sea ice. *Environ. Res. Lett.*, **15**, 124017, https://doi.org/10.1088/1748-9326/abc215.

Zhang, T., T. Wang, Y. Zhao, C. Xu, Y. Feng, and D. Liu, 2021: Drivers of Eurasian spring snow-cover variability. *J. Climate*, **34**, 2037–2052, https://doi.org/10.1175/JCLI-D-20-0413.1.

Zhou, M., and H. Wang, 2014: Late winter sea ice in the Bering Sea: Predictor for maize and rice production in northeast China. *J. Appl. Meteor. Climatol.*, **53**, 1183–1192, https://doi.org/10.1175/JAMC-D-13-0242.1.

Zhuo, W. Q., and Z. N. Jiang, 2020: A possible mechanism for winter sea ice decline over the Bering Sea and its relationship with cold events over North America. *J. Meteor. Res.*, **34**, 575–585, https://doi.org/10.1007/s13351-020-9154-2.

Brought to you by UNIVERSITETSBIBLIOTEKET I | Unauthenticated | Downloaded 04/25/23 11:32 AM UTC